



UPPSALA
UNIVERSITET

UPTEC W 19036

Examensarbete 30 hp
Augusti 2019

Nitrogen Uptake by Vegetation in the Wakkerstroom Wetland, South Africa

Emma Dufbäck

ABSTRACT

Nitrogen Uptake by Vegetation in the Wakkerstroom Wetland, South Africa

Emma Dufbäck

The lack of proper wastewater treatment inhibits the social and economic development in many communities. The South African town Wakkerstroom is an example where wastewater is first treated before it is released. Due to the lack of technical expertise and funding to manage the sewage disposal system, a large part of the wastewater goes directly, without any treatment, into a stream feeding the Wakkerstroom wetland. The wetland purifies the wastewater and provides clean water downstream, thus is indispensable for its detoxification capacity.

One relatively cheap method to determine the absorption capacity of a wetland with respect to nitrogen loading is to investigate the nitrogen uptake by the wetland vegetation. In this study, the nitrogen uptake of the vegetation in the Wakkerstroom wetland during the growing seasons between the years 2000-2018 was investigated by using harvested biomass and its nitrogen content as a proxy. The interannual variability of Net Primary Production (NPP) was calculated using a Light Use Efficiency (LUE) model for the period 2000-2018. The NPP derived with LUE-modelling was compared to NPP based on an end-of season harvest of biomass in March 2019. The nitrogen content and carbon and nitrogen (C:N) ratio were determined in the harvested biomass by carbon and nitrogen content analysis. The annual nitrogen uptake of the growing seasons between the years 2000-2018 was subsequently determined by multiplying the calculated NPP by the fraction of nitrogen found in the harvested material.

The NPP_{tot} based on harvested biomass ($NPP_{harvest}$) towards the end of the growing season 2018/2019 was estimated to be $2.01 \text{ kg}\cdot\text{m}^{-2}\cdot\text{season}^{-1}$. The NPP_{tot} calculated from LUE modelling (NPP_{LUE}) varied between $0.49\text{-}1.64 \text{ kg}\cdot\text{m}^{-2}$ for the growing seasons between 2000-2018. $NPP_{harvest}$ was between 1.2-4 times higher compared to NPP_{LUE} , probably due to overestimation of $NPP_{harvest}$ because of biomass sampling of more than one-year production, or underestimation of NPP_{LUE} due to a low maximum radiation conversion efficiency factor, ϵ_{max} . The community mean nitrogen (N) content found in the biomass harvested aboveground was 1.29 % for the *Phragmites* community and 1.00 % for the *Typha* community. The nitrogen uptake of the vegetation was estimated to vary between $6.10\text{-}20.5 \text{ g N}\cdot\text{m}^{-2}$ per growing season between the years 2000-2018.

Keyword: nitrogen uptake, NPP, wetland, Multi-angle Imaging SpectroRadiometer (MISR), Light Use Efficiency (LUE), remote sensing, *Phragmites australis*, *Typha capensis*, South Africa.

*Department of Ecology and Genetics, Limnology, Uppsala University, Norbyvägen
18D, SE-752 36 Uppsala, ISSN 1401-5765*

REFERAT

Kväveupptag hos växterna i våtmarken i Wakkerstroom, Sydafrika

Emma Dufbäck

Bristen på adekvata reningstekniker för att behandla avloppsvatten hämmar den sociala och ekonomiska utvecklingen i många samhällen. Den sydafrikanska staden Wakkerstroom är ett exempel där avloppsvatten först renas innan det släpps ut. På grund av bristen på teknisk kompetens och finansiering att hantera reningsverket som avlägsnar avloppsvatten så läcker en stor del av det orenade avloppsvattnet ut i en våtmark i Wakkerstroom via en närliggande å. Våtmarken är av regional betydelse för sin reningskapacitet då den renar avloppsvattnet och förser användare nedströms med rent vatten.

En viktig aspekt för att bestämma en våtmarks reningskapacitet med avseende på kväve (N) är att undersöka växternas kväveupptag i våtmarken. Kväveupptaget hos växterna i våtmarken i Wakkerstroom under växtsäsongerna mellan år 2000–2018 undersöktes genom att använda skördad biomassa och dess kväveinnehåll som proxy. Den årliga variabiliteten hos nettoprimärproduktionen (NPP) beräknades genom att använda en LUE (Light Use Efficiency)-modell för perioden 2000-2018. NPP framtaget med LUE-modellering jämfördes med NPP baserat på biomassa skördad i slutet av växtsäsongen i mars 2019. Kväveinnehållet och kol-kväve (C:N) kvoten bestämdes hos den skördade biomassan genom en kol- och kväveanalys. Det årliga kväveupptaget under växtsäsongerna mellan 2000–2018 togs därefter fram genom att multiplicera beräknad NPP med kvävefraktionen erhållen från den skördade biomassan.

NPP_{tot} framtaget med biomassa skördad i slutet av växtsäsongen 2018/2019 (NPP_{biomassa}) uppskattades vara 2,01 kg·m⁻²·säsong⁻¹. NPP_{tot} beräknat med LUE-modellering (NPP_{LUE}) varierade mellan 0,49–1,64 kg·m⁻² under växtsäsongerna mellan år 2000–2018. NPP_{biomassa} var 1,2–4 gånger högre i jämförelse med NPP_{LUE}, vilket troligtvis berodde på att NPP_{biomassa} överskattades på grund av att mer än en årsproduktion av biomassa skördades, eller för att NPP_{LUE} underskattades på grund av ett för lågt värde på den maximala effektivitetsfaktorn ϵ_{\max} valdes. Medelvärde för kväveinnehållet erhållen i biomassan skördad ovanför vattennivån var 1,29 % för *Phragmites*-samhället och 1,00 % för *Typha*-samhället. Kväveupptaget hos växterna varierade mellan 6,10–20,5 g N·m⁻² per växtsäsong mellan år 2000–2018.

Nyckelord: kväveupptag, NPP, våtmark, Multi-angle Imaging SpectroRadiometer (MISR), Light Use Efficiency (LUE), fjärranalys, *Phragmites australis*, *Typha capensis*, Sydafrika.

Institutionen för ekologi och genetik, limnologi, Uppsala universitet, Norbyvägen 18D, SE-752 36 Uppsala, ISSN 1401–5765

PREFACE

This report is part of the MSc degree in Environmental and Water Engineering at Uppsala University and Swedish University of Agricultural Sciences. The study corresponds to 30 Swedish academic credits and was conducted as a Minor Field Study, funded by the Swedish International Development Agency (SIDA). Prof Robert J Scholes at Global Change Institute at the University of the Witwatersrand in Johannesburg was supervisor, and Prof Gesa Weyhenmeyer at the Department of Ecology and Genetics, Limnology, at Uppsala University was subject reader.

I would like to thank my supervisor Prof Robert J Scholes for giving me this incredible opportunity and for invaluable inputs along the way. I would also like to thank my subject reader Prof Gesa Weyhenmeyer for all the important feedback. Many thanks to the MISR team at the University of the Witwatersrand for providing and assisting with the record of FAPAR, and iThemba Labs for performing the C and N content analysis. A big thank you to the locals of Wakkerstroom for showing me such generosity and hospitality. Lastly, I would like to thank my family and friends for their endless support, especially to Markus; your encouragement has meant so much to me!

Emma Dufbäck

Uppsala, June 2019

Copyright © Emma Dufbäck and Department of Ecology and Genetics, Limnology, Uppsala University.

UPTEC W 19036, ISSN 1401–5765

Published digitally at the Department for Earth Sciences, Uppsala University, Uppsala, 2019.

POPULÄRVETENSKAPLIG SAMMANFATTNING

Många samhällen lider av reningstekniker som inte klarar av att rena avloppsvatten, vilket hämmar den sociala och ekonomiska utvecklingen. I den sydafrikanska staden Wakkerstroom är ambitionen att först rena avloppsvattnet innan det släpps ut, men på grund av bristande finansiering och underhåll av reningsverket så läcker orenat avloppsvatten ut i en närliggande våtmark. Våtmarken är av stor betydelse för området då den renar avloppsvattnet från föroreningar och förser användare nedströms med rent vatten. Avloppsvatten innehåller stora mängder näringsämnen, bland annat kväve, vilket avlägsnas i våtmarken genom olika processer. En av dessa processer är genom att växterna i våtmarken tar upp kväve, vilket utgör en viktig del av en våtmarks förmåga att rena vatten.

För att kunna uppskatta kväveupptaget i våtmarken i Wakkerstroom så behövs produktionen av våtmarkens växter samt växternas kväveinnehåll bestämmas. Därefter kunde kväveupptaget bestämmas genom att multiplicera växtproduktionen med kväveinnehållet. För att komma fram till den årliga växtproduktionen, även kallad nettoprimärproduktion (NPP), så skördades växterna i våtmarken (biomassan) i slutet av växtsäsongen för 2018/2019. För att ta reda på NPP för tidigare år så användes observationer från satelliter som fångar upp växters egenskaper, så kallat fjärranalys. Utifrån dessa observationer skapades en modell för att beräkna NPP för växtsäsongerna mellan år 2000–2018. Modellen var en så kallad Light Use Efficiency (LUE)-modell, som beräknar biomassaproduktionen utifrån hur mycket strålning som de tar upp eller ger ifrån sig inom vissa ljusspektrum. NPP som togs fram med LUE-modellen jämfördes med NPP uppskattat från den skördade biomassan för att ta reda på hur väl de överensstämde.

För att undersöka kväveinnehållet hos växterna i våtmarken så analyserades den skördade biomassan för att undersöka dess kol (C)- och kväve (N)-innehåll. Det erhållna kväveinnehållet multiplicerades därefter med NPP som tagits fram med LUE-modellen för att uppskatta det årliga kväveupptaget som våtmarkens växter haft för växtsäsongerna under 2000–2018. Kvoten mellan C och N (C:N) undersöktes då det kan avslöja om växterna i våtmarken kommer att lägga sig på botten efter att de vissnat och bilda torv, eller om de kommer att brytas ned av mikroorganismer och på så sätt släppa tillbaka kvävet som de tagit upp. För att växten ska brytas ned av mikroorganismer så behöver C:N vara lägre än 30, om kvoten istället är högre än 30 är det sannolikt att växterna samlas på botten av våtmarken och på så sätt begraver kvävet som de tagit upp.

NPP som togs fram utifrån den skördade biomassa (NPP_{biomassa}) i slutet av växtsäsongen 2018/2019 uppskattades vara $2,01 \text{ kg}\cdot\text{m}^{-2}\cdot\text{säsong}^{-1}$, vilket avser biomassa i torrsvikt. NPP_{tot} beräknat med LUE-modellering (NPP_{LUE}) varierade mellan $0,49\text{--}1,64 \text{ kg}\cdot\text{m}^{-2}$ under växtsäsongerna mellan år 2000–2018. Det visade sig att NPP_{biomassa} var 1,2–4 gånger högre i jämförelse med NPP_{LUE} . NPP_{biomassa} var troligtvis högre än NPP_{LUE} då biomassan som skördades i enstaka fall var mer än produktionen av endast ett år, vilket överskattade produktionen för den växtsäsongen. Det kan också ha varit så att NPP_{LUE} var för lågt då en av parametrarna i LUE-modellen, den så kallade maximala effektivitetsfaktorn ϵ_{max} , fick ett för lågt värde. ϵ_{max} utgör en viktig del av LUE-modellen då den översätter

mängden energi erhållen från solljus till producerad biomassa. C:N kvoten som togs fram hos växterna i samband med C- och N-analysen påvisade att majoriteten av växterna i våtmarken troligtvis kommer att ansamlas på botten av våtmarken och därmed begrava kvävet som de innehåller. Kväveinnehållet hos växterna som skördades i våtmarken i Wakkerstroom visades sig bestå av 1,29 % kväve för ett växtsamhälle kallat *Phragmites*, och 1,00 % för växtsamhället *Typha*. Utifrån dessa kväveinnehåll beräknades kväveupptaget i våtmarken, vilket visade sig variera mellan 6,10–20,5 g N·m⁻² per växtsäsong mellan år 2000–2018.

DEFINITIONS

δ	Declination angle of the Earth in relation to the Sun at solar noon (Duffie and Beckman 2014).
ϵ	A conversion efficiency factor that translates APAR to final tissue growth or biomass (Running and Zhao 2015).
ϕ	The latitude of the location north or south of the equator (Duffie and Beckman 2014).
ω	The hour angle describes the angular displacement of the Sun of the local meridian, which is negative during the morning and positive in the end of the day (Duffie and Beckman 2014).
Ammonia volatilization	Under basic conditions, the ammonium ion (NH_4^+) is converted to un-ionized ammonia (NH_3) and released as gas (Mitsch, and Gosselink 2015).
Ammonification	See: Mineralization.
Anammox	Nitrite (NO_2^-) and NH_4^+ can under anaerobic conditions convert to nitrogen gas (N_2) through ammonium oxidation using nitrite as oxidant (Mitsch and Gosselink 2015).
APAR	Absorbed Photosynthetically Active Radiation, the quantity of PAR absorbed by leaves (Running and Zhao 2015).
Assimilation, Ammonia	Refers to the process when ammonia (NH_3 or NH_4^+) is taken up by an organism and converted to the organism's biomass (Jaffe 1992).
Biomass	Vegetative material.
C3 plants	Vegetation that produce the three-carbon compound phosphoglyceric acid ($\text{C}_3\text{H}_7\text{O}_7\text{P}$) during the first step of photosynthesis (Sandusky-Aber et al. 2012).
Decomposition	The degradation and breakdown of macrophytes into particulate form (Kadlec and Wallace 2009).
Denitrification	Nitrate (NO_3^-) can act as a terminal electron acceptor under anaerobic conditions by facultative bacteria and transform into N_2 and nitrous oxide (N_2O) (Mitsch, and Gosselink 2015).
DIN	Dissolved inorganic nitrogen.
FAPAR	The Fraction of Absorbed Photosynthetically Active Radiation, which is the fraction of PAR absorbed by green leaves used for photosynthesis (Copernicus Global Land Service 2019-02-20).

f_c	The fraction of carbon found in the wetland vegetation.
f(T_s)	Regulation scalar for low temperatures that lowers ϵ_{\max} (Running and Zhao 2015).
GPP	Gross Primary Production, includes the assimilation of organic matter and the amount used for respiration during a specified time (Kadlec and Wallace 2009).
Hydrophyte	A plant adapted to grow in wet or submersed environments (Germishuizen and Meyer 2003).
Immobilization	Nitrogen is converted from inorganic to organic form through uptake by microorganisms or vegetation (Swift et al. 1979).
LAI	Leaf Area Index, one-sided green leaf area per unit ground area (Diner et al. 2008).
Litter	Dead vegetation that has fallen on the sediment or the ground (Kadlec and Wallace 2009).
LUE model	Light Use Efficiency model used for calculating vegetational production from remote sensing.
Mineralization	The biological conversion of organic bound nitrogen to NH_4^+ is performed by decomposer communities and occurs in both aerobic and anaerobic conditions during degradation of organic material (Mitsch, and Gosselink 2015).
MISR	Multi-angle Imaging SpectroRadiometer, an instrument on board the Terra satellite, collecting aerosol information and land surface products such as FAPAR and albedo (Diner et al. 2008).
NIR	Near-infrared spectral band of the solar spectrum, 700-3000 nanometres (nm) (MISR-HR 2019).
Nitrogen fixation	Biological fixation of N_2 to organic nitrogen occurs in presence of the enzymes nitrogenases which are released from certain microorganisms. The process can be carried out in several places in a wetland as long as the oxygen level is low, such as the surface of leaves and stems of plants and in the rhizosphere of the vegetation etc. (Mitsch, and Gosselink 2015).
NPP_{AG}	Refers to the NPP based on harvested material aboveground or above the water level.
NPP	Net Primary Production, the incorporated organic matter in a plant community for a specific time interval (Kadlec and Wallace 2009).

PAR	Photosynthetically Active Radiation (400-700 nm), one of the components for calculating daily GPP (Running and Zhao 2015).
RF	Root fraction, estimated from harvest of aboveground and belowground biomass.
Sentinel-2	Sentinel-2 imaging mission consists of two satellites, flying in the same orbit, and produces high resolution multispectral images of the surface of the Earth (Sentinel 2019-04-18).
SW_{rad}	The incident shortwave radiation (300-3000 nm) that reaches the surface of the Earth.
SW_{rad,top}	Extra-terrestrial shortwave radiation at the top of the atmosphere (Almorox et al. 2004).
VIS	Visible spectral band of the solar spectrum, 300-700 nm (MISR-HR 2019).
Vlei	Afrikaans term for a wetland, used in parts of southern Africa (Sandusky-Aber et al. 2012).

TABLE OF CONTENTS

ABSTRACT.....	i
REFERAT.....	ii
PREFACE.....	iii
POPULÄRVETENSKAPLIG SAMMANFATTNING.....	iv
DEFINITIONS.....	vi
1. INTRODUCTION.....	1
1.1 MAIN OBJECTIVE OF THE STUDY AND SPECIFIC RESEARCH QUESTIONS	2
2. BACKGROUND.....	2
2.1 WETLANDS FOR TREATING WASTEWATER.....	2
2.1.1 The store-release effect of nitrogen maintained by the wetland vegetation.....	4
2.2 METHODS FOR ESTIMATING NPP AND NITROGEN CONTENT.....	5
2.2.1 Biomass sampling.....	5
2.2.2 LUE modelling based on remotely sensed data.....	7
3. MATERIALS AND METHODS.....	11
3.1 STUDY SITE.....	11
3.2 HARVESTED BIOMASS.....	12
3.2.1 Biomass sampling.....	12
3.2.2 Carbon and nitrogen content analysis.....	16
3.2.3 Estimating NPP.....	19
3.3 LUE MODELLING.....	21
3.3.1 FAPAR derived from MISR.....	21
3.3.2 Calculating PAR.....	23
3.3.3 Conversion efficiency factor ϵ	24
3.3.4 Calculating NPP.....	26
3.4 METHOD COMPARISON OF NPP, AND CALCULATION OF NITROGEN UPTAKE.....	27
4. RESULTS.....	28
4.1 CARBON AND NITROGEN CONTENT IN WETLAND VEGETATION.....	28
4.2 NPP.....	29
4.2.1 NPP based on harvested biomass.....	29
4.2.2 NPP based on LUE modelling.....	30
4.2.3 Comparison of NPP from harvested biomass and NPP from LUE modelling....	31
4.3 NITROGEN UPTAKE OF THE WETLAND VEGETATION.....	32
5. DISCUSSION.....	34
5.1 NPP.....	34
5.1.1 NPP estimated from harvested biomass.....	34

5.1.2	NPP calculated from LUE modelling.....	35
5.1.3	Comparison of the two methods for obtaining NPP.....	37
5.2	CARBON AND NITROGEN CONTENT IN THE WETLAND VEGETATION	38
5.2.1	Nitrogen uptake	39
6.	CONCLUSIONS.....	40
	REFERENCES.....	41
	APPENDIX.....	46
	A. BIOMASS SAMPLING.....	46
	B. FAPAR	49
	C. PAR	51
	D. CONVERSION EFFICIENCY FACTOR ϵ	54
	E. NPP	55
	F. CARBON AND NITROGEN CONTENT	56
	G. CLIMATOLOGY DATA.....	58
	H. WEATHER STATIONS	59

1. INTRODUCTION

Four-fifths of the wastewater in the world flows back into ecosystems without being treated or reused (UNESCO 2017). The lack of proper wastewater treatment inhibits the social and economic development in many communities. One management strategy which is particularly useful for geographical regions suffering from water stress is to first treat and then to reuse wastewater (United Nations 2018). Such treatment strategies are common in many countries, among them South Africa. The South African town Wakkerstroom is an example where wastewater is first treated before it is released. The treated wastewater is held in ponds, where some nitrogen is lost through denitrification, and some by drainage to the groundwater, from where it discharges into a stream feeding an adjacent wetland, known as the Wakkerstroom vlei. Due to the lack of technical expertise and funding to manage the sewage disposal system, a large part of the wastewater goes directly, without any treatment, into the stream feeding the wetland. There is no official record of how long this leakage of wastewater has existed, but it is estimated to have been occurring since the installation of the sewage system, which took place approximately 10 years ago (Scholes 2018¹). The Wakkerstroom vlei purifies the wastewater and provides clean water downstream, thus is indispensable for its detoxification capacity (Ellery and Joubert 2013).

Untreated wastewater has high concentrations of organic matter and nutrients, such as nitrogen. Wetlands are known for their ability to remove nutrients from waters by an efficient absorption capacity. Thus, wetlands can purify waters (Mitsch, and Gosselink 2015; Wardrop et al. 2016). One aspect to determine the absorption capacity of a wetland with respect to nitrogen loading is to investigate the nitrogen uptake by the wetland vegetation. This information is essential for further investigation regarding the absorption capacity of the wetland.

The investigation of the nitrogen uptake by the wetland vegetation can be done by estimating the Net Primary Production (NPP) and the nitrogen content of the standing biomass at the end of the growing season, within a given area. NPP is defined as the biomass accumulated by the vegetation during a specified time interval and can be measured by harvesting biomass (Kadlec and Wallace 2009). Knowing the nitrogen fraction of the harvested biomass and the NPP of the wetland, the nitrogen uptake can be determined by multiplying the fraction of nitrogen with the NPP. It is also of importance to determine the carbon and nitrogen ratio (C:N) of the harvested biomass to know if the nitrogen is likely to be sequestered or mineralized following its death; the lower C:N ratio, the greater possibility of net mineralization (Eriksson et al. 2011).

Another way of determining the NPP is to use a Light Use Efficiency (LUE) model based on satellite observations of the phenology of leaf exposure. For determining NPP, remotely sensed data such as the Fraction of Absorbed Photosynthetically Active Radiation (FAPAR) is required (Running and Zhao 2015). An instrument that provides FAPAR is the Multi-angle Imaging SpectroRadiometer (MISR) (Verstraete et al. 2012).

¹ Personal communication 2018, Prof RJ Scholes, University of the Witwatersrand.

Due to the MISR instrument's multi-angular sensor, it is a unique instrument providing new information about the Earth's climate and land surface (Jet propulsion Laboratory 2019-03-27).

1.1 MAIN OBJECTIVE OF THE STUDY AND SPECIFIC RESEARCH QUESTIONS

The main objective of this study was to contribute to the quantification of the absorption capacity of the Wakkerstroom wetland with regards to the nitrogen uptake by the wetland vegetation. To reach this goal the nitrogen uptake of the vegetation in the Wakkerstroom wetland during the 2018-2019 growing season was quantified by using harvested biomass and its nitrogen content as a proxy. The interannual variability of NPP was calculated using a LUE model for the period 2000-2018, based on FAPAR derived every few days from the MISR instrument. The satellite-derived NPP was compared to NPP based on an end-of season harvest of biomass in March 2019. The nitrogen content and C:N ratio was determined in the harvested biomass by carbon and nitrogen content analysis, conducted by iThemba Labs at the University of the Witwatersrand. The annual nitrogen uptake of the growing seasons between the years 2000-2018 was subsequently determined by multiplying the calculated NPP by the fraction of nitrogen found in the harvested material.

The specific research questions for this study were:

- What is the estimated NPP based on harvest of aboveground material at the end of the growing season, in March 2019?
- What is the mean and variance of annual NPP of the wetland, estimated by remote sensing, for the growing seasons between the years 2000-2018?
- What is the aboveground and belowground nitrogen content and the C:N ratio in the end-of season standing biomass of the wetland harvested in March 2019?
- What is the estimated nitrogen uptake of the vegetation, and its interannual variation, for the growing seasons between the years 2000-2018 based on calculated NPP and structural nitrogen content in the harvested biomass?

2. BACKGROUND

2.1 WETLANDS FOR TREATING WASTEWATER

A wetland used for improving water quality is referred to as a treatment wetland. There are three groups of treatment wetlands: natural, surface-flow constructed, and subsurface-flow constructed (Mitsch and Gosselink 2015). The wetland type of the Wakkerstroom vlei is a naturally occurring wetland, henceforth is the term wetland in this study referring to a natural wetland.

Wetlands are found all over the world, with the highest density in boreal and sub-boreal regions in the Northern Hemisphere, and the second highest density in the tropics and subtropics (Sandusky-Aber et al. 2012). There are several types of wetlands, but they all are defined by the presence of water in the root zone or at the surface, the unique composition of the soil due to accumulation of decomposing vegetation, and the variety of animals and plants adapted to the wet conditions. A wetland is an ecosystem including properties from both terrestrial and aquatic environments (Mitsch, and Gosselink 2015). They provide several ecosystem services for the modern society such as supplying fresh water, impeding flooding, sustaining irrigated agriculture, supporting wildlife and vegetation, recharging aquifers etc. They are also essential for the overall functioning of the Earth's system, as they are responsible for material and energy transitions (Sandusky-Aber et al. 2012).

Wetlands are also known to be efficient in improving water quality. Compounds such as heavy metals, suspended sediments, excess nutrients, particulate matter etc. can get trapped or removed from the water through different processes (Sandusky-Aber et al. 2012). In a wetland environment, nitrogen occurs in various forms ranging from organic nitrogen to the mineralized forms nitrate (NO_3^-), nitrite (NO_2^-), ammonia (NH_4^+ and NH_3), nitrous oxide (N_2O) and nitrogen gas (N_2), making mechanisms regarding nitrogen complex. The processes found in wetlands regarding removing or storing excessive nitrogen are:

- **physical processes.** The compounds are trapped by the surface of roots and stems (Sandusky-Aber et al. 2012) or exported through groundwater flow. The latter is possible for the mobile compound NO_3^- . Settling of particulate nitrogen resulting in sedimentation is also a possible removal mechanism. Assimilated nitrogen can be physically removed by harvest of the wetland vegetation (Kadlec and Wallace 2009), or be released to the atmosphere as N_2O , NH_3 , NO_x or HNO_3 when the biomass burns, according to Cofer et al. (1990).
- **chemical processes,** which include ion exchange and adsorption (Sandusky-Aber et al. 2012). NH_4^+ is likely to get immobilized onto negatively charged soil particles through ion exchange. Chemical processes like denitrification, anammox and ammonia volatilization play important roles regarding nitrogen removal. Denitrification is, along with reduction to NH_3 , the major pathways causing nitrogen loss in wetlands (Mitsch and Gosselink 2015).
- **biological processes.** Mineralized nitrogen is removed from the water and transformed to organic material through uptake by vegetation, algae and microbes (Sandusky-Aber et al. 2012). The nitrogen is released back into the water through nitrogen mineralization (Mitsch and Gosselink 2015). The nutrient can get stored long-term through the partial decomposition of organic matter and formation of peat (Sandusky-Aber et al. 2012).

2.1.1 The store-release effect of nitrogen maintained by the wetland vegetation

The nitrogen needs to be bioavailable to the vegetation to be assimilated. Roots are generally not permeable to organic compounds and therefore the majority of nitrogen is absorbed as dissolved inorganic nitrogen (DIN) (Swift et al. 1979). From a short-term (within season) perspective, wetland vegetation is a removal mechanism regarding nitrogen as it assimilates DIN when it grows and thus removes DIN from the water, improving the water quality. Biomass is produced during the growing season and uptake of DIN occurs via the roots, which the above- and belowground parts of the plant subsequently assimilate into nitrogen-containing organic compounds. The most common forms of DIN to get absorbed by vegetation are NH_4^+ and NO_3^- (Kadlec and Wallace 2009). Organic nitrogen generally makes up 1-7 % of the total dry mass of plants, but it varies depending on the type of vegetation and environmental conditions. The nitrogen content also varies for the different plant parts (Kadlec and Wallace 2009).

From a longer-term perspective (annual and longer), vegetation has a store-release effect rather than a removal effect with respect to nitrogen. Organic nitrogen is stored in the vegetation throughout the growth cycle. Once the vegetation dies it turns to litter and the organic nitrogen is released into the surrounding waters through mineralization. The decay of organic material is important for the cycling of nutrients as the majority of the assimilated nitrogen is released into the water as DIN. However, not all of the litter is fully decomposed, some is buried and undergoes peat formation, while some exits the system as particulate organic nitrogen or dissolved organic nitrogen in the water leaving the system. The burial of litter creates stable accretions containing organic nitrogen, thus providing a storage mechanism (Kadlec and Wallace 2009).

According to Kadlec and Wallace (2009), decomposition of litter occurs at a range of rates, depending on environmental factors and the composition of the organic matter. One factor controlling litter degradability is the availability of nutrients and energy sources for the decomposer organisms. Litter is decomposed by decomposer communities consisting of microorganisms and invertebrates. These communities feed on the litter and utilize nutrients and energy sources, in the form of carbon compounds, for their growth (Swift et al. 1979). Decomposers extract enzymes which catalyse the decomposition of organic molecules. The decomposers use carbon for their respiration, hence oxidising carbon to carbon dioxide (CO_2), and convert organic nitrogen to DIN (Eriksson et al. 2011).

During the decomposition of litter, organic nitrogen is transformed to DIN through mineralization. Subsequently, a part of the DIN is taken up by decomposers, vegetation and other organisms for growth, thus inducing immobilization in microbial biomass, or re-entry into the plant assimilation system described above (Eriksson et al. 2011). The availability of DIN determines net mineralization, which denotes the degree to which mineralization exceeds immobilisation. Net mineralization occurs when there is enough DIN for the decomposers to utilize, hence when the DIN no longer is limiting to the decomposer communities (Swift et al. 1979).

There is generally an abundance of energy in the litter, while organic nitrogen very often is the limiting factor in the mineralization process (Swift et al. 1979). The relationship between the energy source and nitrogen is commonly written as the C:N ratio, where carbon represents the energy source. Typically, the C:N ratio in the litter needs to be less than 30 for mineralization to occur (van der Walk 2006).

2.2 METHODS FOR ESTIMATING NPP AND NITROGEN CONTENT

In order to determine the nitrogen uptake by the wetland vegetation, estimates on NPP of the wetland and the fraction of organic nitrogen in the wetland plant community are needed. Biomass sampling within a given area is one method for estimating NPP and the nitrogen content (Kadlec and Wallace 2009). Another way of estimating NPP is to use a LUE model based on satellite observations of the phenology of leaf exposure. The latter method has some advantages compared to harvesting biomass as it measures at larger spatial scales and continuously over long periods of time.

2.2.1 Biomass sampling

Ground-based sampling is a good method for investigating a wetland's flora and fauna (Sandusky-Aber et al. 2012). For estimating the annual NPP and the nitrogen content in the vegetation, the annual standing stock of live and dead vegetation is harvested at the end of the growing season (Kadlec and Wallace 2009).

The vegetation compartments commonly sampled are aboveground biomass, standing dead, litter and belowground rhizomes and roots. In this case, the term aboveground (AG) refers to the standing stock present above the water level, while belowground (BG) is the biomass beneath the water level including the roots and rhizomes. The sampling of belowground material is very often difficult, resulting in a neglect of this particular biomass component (Kadlec and Wallace 2009). Single-time harvesting of biomass in order to estimate the annual NPP is generally an underestimate of the true production, due to unmeasured production losses because of grazing, shedding of plant parts, diseases etc. (van der Walk 2006).

When estimating NPP based on harvested aboveground plant material, one option is to simply neglect the belowground biomass, which results in a large underestimation of the NPP. Another option is to combine aboveground NPP (NPP_{AG}) with the root fraction (RF) of the dried biomass for estimating the total NPP (NPP_{tot}) (Eq. 1). RF is computed from biomass harvested both aboveground and belowground (Eq. 2).

$$NPP_{AG} = NPP_{tot}(1 - RF) \leftrightarrow NPP_{tot} = \frac{NPP_{AG}}{1 - RF} \text{ [kg}\cdot\text{season}^{-1}] \quad (1)$$

$$RF = \frac{BG}{AG + BG} [-] \quad (2)$$

The NPP_{AG} for the area of interest, representing one growing season, is estimated from the mean dry mass per area unit (\bar{m} [$kg \cdot m^{-2} \cdot season^{-1}$]) of the harvested material multiplied by the area (A [m^2]) (Eq. 3).

$$NPP_{AG} = \bar{m} \cdot A \text{ [kg} \cdot \text{season}^{-1}] \quad (3)$$

Biomass sampling depends on the species sampled. In this particular study, *Phragmites australis* (*Phragmites*) and *Typha capensis* (*Typha*) (Fig. 1) were the dominant plant species in the almost mono-dominant vegetation communities found in the Wakkerstroom vlei (Ellery and Joubert 2013; Scholes 2019²). Both of these species are emergent C3 hydrophytes, which means that they produce the three-carbon compound phosphoglyceric acid during the first step of photosynthesis. Wetland vegetation and aquatic plants belongs to the group hydrophytes, which have adapted to thrive during the extreme circumstances found in wetlands such as flooding, lack of oxygen and nutrients, low pH etc. (Sandusky-Aber et al. 2013). Emergent hydrophytes are vegetation that grows on submersed or water-saturated soils with the aboveground plant part emerging above the water line (Kadlec and Wallace 2009). *Phragmites australis*, known as common reed, is an indigenous plant species in South Africa. It is a tall perennial reed found in tropical and temperate wetlands (Sandusky-Aber et al. 2013). Its stem is hollow, robust (Packer et al. 2017) and can measure up to 4 m (Germishuizen and Meyer 2003). In treatment wetlands, reed-like grasses such as *Phragmites* are commonly used for improving the water quality (Mitsch, and Gosselink 2015). *Typha*, commonly referred to as bulrush, is a perennial species reaching a height of 2 m (Germishuizen and Meyer 2003). It is recognized by its brown cylindrical velvet-spikes and is very common in southern Africa (South African National Biodiversity Institute 2007).

² Personal communication 2019, Prof RJ Scholes, University of the Witwatersrand.



Figure 1. *Phragmites australis* (left) and *Typha capensis* (right).

2.2.2 LUE modelling based on remotely sensed data

Ground-based investigations of wetlands can be difficult and labour intensive. Another method for gathering information about wetlands and vegetation is to use satellite observations. Satellite imagery and aerial photography, so called remote sensing, collects information from a distance with various types of detectors or cameras. Visible and invisible radiation is emitted or reflected from different objects on the ground and collected by the detectors (Sandusky-Aber et al. 2012). The data derived from remote sensing can be used in LUE models for estimating vegetation production (Liang et al. 2012).

The theory behind the idea to use land surface indices for estimating NPP is based on the following assumptions:

- 1) The NPP of vegetation is related to the amount of solar energy absorbed by plants,
- 2) a relation exists between spectral vegetation indices derived from satellites and absorbed solar energy, and
- 3) the actual conversion efficiency is lower than the optimum theoretical value due to biophysical constraints on growth other than light-harvesting, such as water, temperature and nutrient limitation (Running and Zhao 2015).

There are many remotely sensed spectral indices of vegetation. One of those is FAPAR which is the fraction of absorbed solar radiation that green leaves use for photosynthesis, thus only referring to the green canopy of plants (Copernicus Global Land Service 2019-02-20). FAPAR has the advantage that it is biophysically defined, and thus assumption 2) above is directly met. Gross Primary Production (GPP), which is the assimilated biomass and the mass used for respiration during a specified time (Kadlec and Wallace 2009), is calculated from Absorbed Photosynthetically Active Radiation (APAR) and the radiation use efficiency constant ε ($\text{g C}\cdot\text{MJ}^{-1}$). APAR is equal to FAPAR multiplied with the daily incident of Photosynthetically Active Radiation (PAR) (Running et al. 2004) (Eq. 4).

$$\text{GPP} = \text{APAR} \cdot \varepsilon \leftrightarrow \text{GPP} = \text{FAPAR} \cdot \text{PAR} \cdot \varepsilon \quad [\text{g C}\cdot\text{m}^{-2}\cdot\text{day}^{-1}] \quad (4)$$

PAR is the solar radiation between 400-700 nm that is absorbed by ecosystems (LAADS DAAC 2019) and it is estimated from incident shortwave radiation (SW_{rad}) (Running and Zhao 2015) (Eq. 5).

$$\text{PAR} = \text{SW}_{\text{rad}} \cdot 0.45 \quad [\text{MJ}\cdot\text{m}^{-2}\cdot\text{day}^{-1}] \quad (5)$$

SW_{rad} on a plane horizontal surface on Earth can be estimated from the extra-terrestrial solar radiation at the top of the atmosphere ($\text{SW}_{\text{rad,top}}$). The solar radiation reaching the surface of the Earth has been attenuated due to atmospheric scattering, which allows radiation to change directions when colliding with molecules and particles, and atmospheric absorption, where ozone, carbon dioxide and water vapour are the major molecules absorbing radiation in the solar energy spectrum. The Ångström-PreScott equation can be used for calculating SW_{rad} (Eq. 6), where a and b are regression constants depending on the location, n is the number of daily hours of sunshine and N is the number of hours between sunrise and sunset (Duffie and Beckman 2014). The regression constants, a and b, are assumed to be, respectively, 0.2 and 0.5 based on the study by Mulaudzi et al. (2013) for the Vhembe region in the Limpopo province, South Africa.

$$\frac{\text{SW}_{\text{rad}}}{\text{SW}_{\text{rad,top}}} = a + b \cdot \frac{n}{N} \rightarrow \text{SW}_{\text{rad}} = \text{SW}_{\text{rad,top}} \left(0.2 + 0.5 \cdot \frac{n}{N} \right) \quad [-] \quad (6)$$

The maximum hours of sunshine, N, can be calculated using Eq. 7, where ω is the hour angle (Duffie and Beckman 2014), described more in detail below.

$$N = \frac{2\omega}{15} \cdot \frac{180}{\pi} \quad [-] \quad (7)$$

The $\text{SW}_{\text{rad,top}}$ is a function of latitude and the day of year (Eq. 8), where I_{sc} is the solar constant with the value $1367 \text{ W}\cdot\text{m}^{-2}$, d is the Julian day of the year with January the 1st as number 1, ϕ is the latitude of the location in radians, δ is the declination angle in radians and ω is the hour angle in radians. ϕ , δ and ω are calculated with Eq. 9-11, where L is the latitude in degrees (ITACA 2019-04-19).

$$\text{SW}_{\text{rad,top}} = \frac{86400 \cdot I_{\text{sc}}}{\pi} \left(1 + 0.034 \cdot \cos\left(\frac{2\pi d}{365.25}\right) \right) \cdot (\cos(\phi) \cdot \cos(\delta) \cdot \sin(\omega) + \omega \cdot \sin(\phi) \cdot \sin(\delta)) \quad [\text{J}\cdot\text{m}^{-2}\cdot\text{day}^{-1}] \quad (8)$$

$$\delta = -\frac{23.45\pi}{180} \cos\left(\frac{360\pi}{365 \cdot 180} (d + 10)\right) \text{ [rad]} \quad (9)$$

$$\phi = -\frac{23.45 \cdot L \cdot \pi}{180} \text{ [rad]} \quad (10)$$

$$\omega = \arccos(-\tan(\phi) \tan(\delta)) \text{ [rad]} \quad (11)$$

For calculating GPP, the conversion efficiency factor ϵ is required, which converts APAR to carbon assimilated. There are several methods for determining the value of ϵ . This project is based on the values used in the LUE model underlying the MOD17 GPP product produced by NASA. The MOD17 algorithm produces records of GPP from surface indices derived with the Moderate Resolution Imaging Spectroradiometer (MODIS) aboard the Terra and Aqua satellites. The principal for obtaining the conversion efficiency is that ϵ varies for different types of vegetation and climate conditions (Running and Zhao 2015). The maximum value of the conversion efficiency (ϵ_{\max}) for a given vegetation type is attenuated due to stress factors, such as low temperatures and water-stress (Numerical Terradynamic Simulation Group 2019-02-21). ϵ is the product of ϵ_{\max} , $f(T_s)$ and $f(W_s)$ (Eq. 12), where the function f varies from 0 to 1, and T_s and W_s are downward regulation scalars for low temperatures and water-stress, respectively (Yuan et al. 2014). In the case of permanently wet wetlands, such as the Wakkerstroom vlei, the water stress scalar falls away.

$$\epsilon = \epsilon_{\max} \cdot f(T_s) \cdot f(W_s) \text{ [g C} \cdot \text{MJ}^{-1}] \quad (12)$$

NPP is equal to GPP minus respiration. The respiration is estimated to amount to approximately 50 % of the GPP (Eq. 13) (Chapin et al. 2011; Liang et al. 2012).

$$\text{NPP} = 0.5 \cdot \text{GPP} \text{ [g C} \cdot \text{m}^{-2} \cdot \text{day}^{-1}] \quad (13)$$

To be able to compare calculated NPP from remote sensing with NPP based on dry harvested biomass, the C content of the vegetation is required, expressed as the fraction of C (f_c) (Eq. 14).

$$\text{NPP}_{\text{tot}} = \frac{\text{NPP}}{f_c} \text{ [g} \cdot \text{m}^{-2} \cdot \text{day}^{-1}] \quad (14)$$

The FAPAR used for calculating NPP is favourably obtained from the MISR instrument. Due to the instrument's capture of reflectances from nine different angles, the record of FAPAR is more accurate than most imaging space-borne instruments. Most other orbiting instruments are equipped with a sensor measuring land surfaces from one direction (Atmospheric Science Data Center 2019). Each camera of the MISR instrument is equipped for capturing data in four spectral bands, three within visible radiation (VIS), blue (446.4 nm), green (557.5 nm), red (671.7 nm) radiation, and one within near-infrared radiation (NIR) (866.4 nm) (Verstraete et al. 2012).

The design purpose of the MISR instrument is to collect information about aerosols and clouds along with capturing spectral indices from the surface of the Earth (Liu et al. 2017). The instrument was developed by Jet Propulsion Laboratory and is hosted on the NASA's Terra platform. It has been measuring continuously since February 2000 to present.

Products derived from MISR are stored as full orbits, but datasets for smaller regions can be ordered in blocks with areas of $385 \times 140.8 \text{ km}^2$. The instrument orbits around the Earth 14.6 times a day, passing over the equator at 10:30 AM local time on a descending limb, and follows a 16-day repeat cycle, which results in 233 different paths per cycle. Since the satellite travels with constant speed in a circular orbit, the equatorial crossings for the paths sampled the same day are separated by a constant distance, which is by about 26 degrees, equal to 2745 km at the equator. Products obtained from the same path refer to geographical areas observed from the same angle, while products from different paths give temporal and spatial coverage, where each path consist of 180 blocks (Fig. 2) (Verstraete et al. 2012). The record of FAPAR, and other MISR parameters, are freely available from NASA Langley Distributed Active Archive Center (DAAC) (MISR 2018).

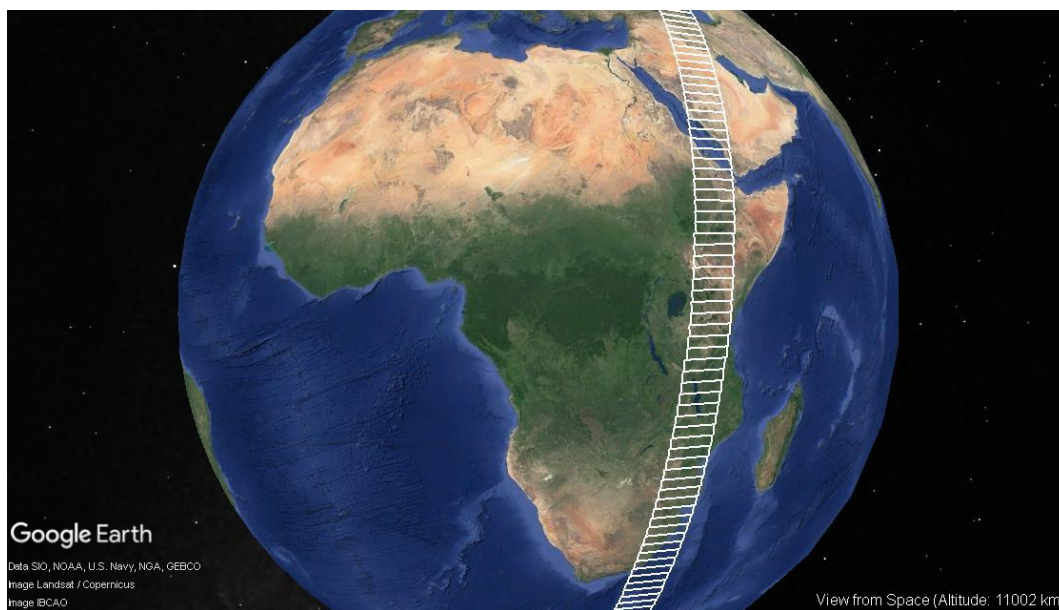


Figure 2. The MISR instrument orbits around the Earth 14.6 times a day in 16-days cycles, which results in 233 different paths. On the picture is path 168 visible with its 180 blocks © Google Earth (2019c).

The MISR instrument allows the generation of several land surface products in addition to the atmospheric products for which it was intended. FAPAR as retrieved by the MISR Level 2 (L2) Land Product and is derived from Leaf Area Index (LAI). The cameras have a ground sampling distance of 275 m, and LAI is collected with 4 samples x 4 line averages, thus resulting in a sampling coverage of 1.1 km. In most products based on single-angle spectral measurements, LAI is calculated based on an empirical relationship with a derived spectral index such as NDVI, and FAPAR is estimated based on determined biome type and LAI for a certain area (Diner et al. 2008). In contrast, the MISR data can be processed in the MISR-High Resolution (HR) processing system, as operated in the Global Change Institute of the University of the Witwatersrand. MISR-HR re-analyses L2 data and generates high level data over terrestrial surfaces with a

ground sampling distance of 275 m, instead of the 1.1 km of the standard MISR products (MISR-HR 2018). The L2 Land Product is one of the MISR products required for the MISR-HR to generate the following high level output (MISR-HR 2015a):

- Rahman-Pinty-Verstraete (RPV) product: model parameters describing the anisotropy of the surface, uncertainties of the parameters and the cost function,
- Joint Research Centre Two-stream Inversion Package (JRC TIP) product: surface property products, such as FAPAR. The JRC TIP is derived from the RPV product (MISR-HR 2015b).

The cost function is an important parameter when using FAPAR. It indicates the quality of the retrieved data; a high value implies a divergence between the data and the model, while a low value represents a good fit (MISR-HR 2019).

3. MATERIALS AND METHODS

3.1 STUDY SITE

The focus of this study has been the tropical wetland immediately west of the town of Wakkerstroom, in Mpumalanga province, South Africa, known locally as the Wakkerstroom vlei (27°20'49.2''S; 30°08'2.4''E) (Fig. 3). It is located in the upper regions of the Tugela catchment, and has a permanently-flooded area of approximately 400 hectares, and seasonally-wet fringes adding a further 150 hectares. The wetland and its surroundings are preserved by the Wakkerstroom Natural Heritage Association (Oellerman 1994). The majority of the wetland is owned by the Wakkerstroom municipality and is leased out for grazing (Kotze et al. 1994). The northern part of the wetland is connected to the Wakkerstroom river, which is the main water input. The Thaka river is formed south of the wetland and leads to the Zaaihoek Dam (Ellery and Joubert 2013). The wetland is highly valued for the nesting grounds it provides for threatened bird species. Due to its purification properties, the wetland is of regional importance for the water supply it provides for downstream users (Kotze et al. 1994).

The Wakkerstroom town sewage disposal system is located northeast of the wetland. Due to the lack of maintenance, the wastewater is frequently overflowed, thus leaking untreated wastewater into the surrounding waters, which finally reaches the wetland via the Wakkerstroom river. The contaminated water flows through the wetland before reaching the Thaka river.

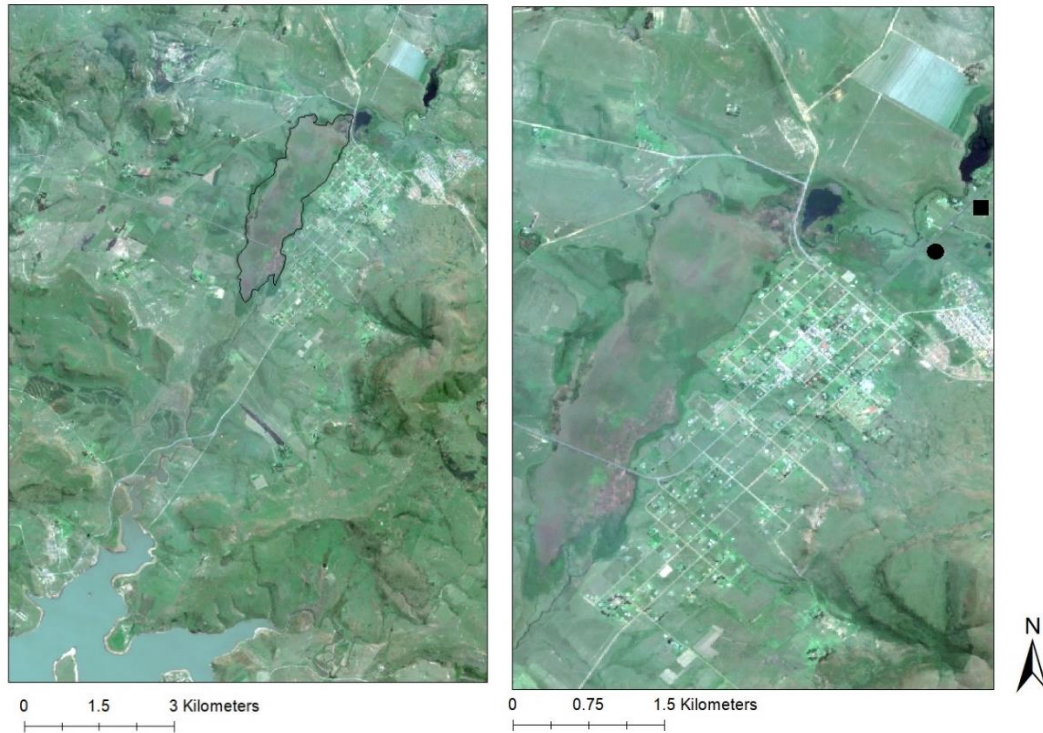


Figure 3. The black line enclosures the Wakkerstroom vlei, located west of the town of Wakkerstroom. Part of the Zaaihoek dam is visible in the southwest corner of the map (left). The sewage disposal system is located northeast of the wetland and is marked with a black square. The pump station, where the leaking of wastewater occurs, is located southwest of the sewage disposal system and is marked with a black dot (right). © Copernicus Sentinel Data (2019).

3.2 HARVESTED BIOMASS

3.2.1 Biomass sampling

The harvest of biomass took place towards the end of the growing season in South Africa, during the time period 10-19 March 2019 at nine locations in the Wakkerstroom wetland (Fig. 4). At the time of sampling, all wetland plants were fully green, but two weeks later they had begun to die and turn brown as a result of the first frosts in this high-altitude location. The aim was to sample at different locations around the wetland. Due to difficulties of reaching the interior of the wetland, it was not sampled.



Figure 4. Biomass sampling were performed at nine different locations at the Wakkerstroom wetland. For the latitude and longitude of each location, see Tab. A1 in Appendix A. © Copernicus Sentinel Data (2019).

The main plant communities in the wetland, respectively dominated by the species *Phragmites* and *Typha*, were sampled separately 2-3 times at each sampling location. The criteria for the sampling was that the roots of the plant community of interest had to be submersed under water. An estimation on site of the presence of each plant community was made to know approximately how many samples were required for each community. The harvested biomass consisted of twenty samples of the *Phragmites* community and five samples of *Typha* community (Tab. 1).

Table 1. The sample number (nr) of *Phragmites* and *Typha* communities sampled at each location.

Location	Sample nr of <i>Phragmites</i>	Sample nr of <i>Typha</i>
1	1	1, 5
2	2	2
3	-	3, 4

4	3, 4, 5	-
5	6, 7, 8	-
6	9, 10, 11	-
7	12, 13, 14	-
8	15, 16, 17	-
9	18, 19, 20	-

A frame with an area of 0.5 x 0.5 m (0.25 m²) was used for harvesting the biomass. The frame was placed on a site predominated by the vegetation of interest and a bar with 0.5-meter markings was used for measuring the water depth at the sampling site. All the above-water biomass within the frame was cut with secateurs, including vegetation that did not belong to the species of interest, and collected in a bucket (Fig. 5).



Figure 5. A frame with an area of 0.25 m² was used for collecting the vegetation of interest. The biomass was encircled with the frame and the water depth at the sampling site was measured with a bar with 0.5-meter markings (left). The biomass above the water within the frame was cut with secateurs and collected in a bucket (right).

The harvested biomass was removed from the bucket and packed in several paper bags marked with the species community, sample number and bag number (Fig. 6). For example: T 3/4 stands for *Typha*, sample number 3 and bag number 4. Sites where a fire had occurred the previous growing season were favourable as those places only contained first year biomass. If no such place existed at a certain location, a site that included both living and dead vegetation was chosen and the standing vegetation within the frame was collected. The wet mass of each sample was thereafter measured.



Figure 6. The sampled biomass was stored in paper bags marked with species community, sample number and bag number.

Sample number 1-5 of *Phragmites* and 1-3 of *Typha* were placed in a solar drying oven for drying. The oven was similar to a greenhouse and equipped with a fan for removing the moisture inside the oven (Fig. 7). The samples were dried for 5-12 days, depending on the sampling dates, and their mass were measured daily during that time. It was not possible to dry all the samples due to lack of space in the oven and shortage of time. The mass of some of the dried samples increased after a few days in the oven, which might have occurred due to high moisture content inside the oven, allowing the paper bags to absorb moisture. A mean dry matter (DM) content was calculated for each plant community by dividing the lowest dry mass with the wet mass of the samples.



Figure 7. Five samples of *Phragmites* and three samples of *Typha* were dried for 5-12 days in a drying oven equipped with a fan.

To estimate the root fraction (RF), biomass above and below the water level was sampled at location 1 for each plant community. Five samples were harvested for *Phragmites* and three for *Typha*. The aim was to locate one stem of the vegetation of interest, cut it off at the surface of the water (referred to as aboveground, AG_{RF}) and then follow the remaining stem down to its roots and rhizomes (referred to as belowground, BG). The BG material was collected by removing the roots from the ground with a spade. The BG biomass was roughly rinsed, if covered with mud, and the biomass for the AG_{RF} and BG material was stored in separate paper bags. The wet mass of the samples was measured (Tab. A4, Appendix A). However, a complete harvest was very difficult to achieve as the roots were occasionally deep in the sediment and it was difficult to distinguish which roots belonged to which stem. It was also difficult to collect all biomass in the form of roots and rhizomes, and to remove all the mud.

The BG samples were dried at 60 °C in an oven at the University of the Witwatersrand for three days and the dry mass of the samples was measured. For calculating RF for each plant community, the dry mass of the samples was required. Since measured dry mass did not exist for most of the AB_{RF} biomass, the measured wet mass was converted to a dry mass by multiplying by the mean DM content of that plant community, based on the samples for which a DM did exist.

3.2.2 Carbon and nitrogen content analysis

To get a representative sample of the harvested biomass for the carbon and nitrogen (C and N) content analysis, five paper bags of each plant community were randomly chosen (Tab. 2), and the biomass within the bags was cut into pieces of 2-3 cm (Fig. 8). The biomass was dried in an oven at 60 °C at the University of the Witwatersrand for one day. It was also of interest to know the C and N content in the belowground biomass. Three bags of the biomass sampled belowground for the estimation of RF were randomly chosen for each community. This biomass was also cut in pieces of 2-3 cm, but instead of storing

the shredded biomass in separate bags, the BG biomass was accidentally mixed in one bag per plant community, which could not be separated afterwards.

Table 2. Five bags for each plant community were randomly chosen for the harvested biomass while three bags were chosen for the belowground biomass.

Plant community	Harvested biomass (sample nr/bag nr)	Belowground biomass (sample nr/bag nr)
<i>Phragmites</i>	1/5	1/1
	7/1	2/1
	9/5	4/1
	13/1	-
	19/2	-
<i>Typha</i>	1/1	3/1
	2/3	4/1
	3/2	5/2
	4/1	-
	5/3	-



Figure 8. The biomass was cut with secateurs into pieces of 2-3 cm.

The shredded samples from the harvested biomass were mixed before a handful of one subsample from each bag was collected. Five subsamples for the BG biomass were collected in the same manner (Tab. 3). The subsamples were ground in a plant mill, one by one, and stored in a marked glass jar with lid for each subsample. The plant mill was cleaned between the grinding sessions. The subsamples were thereafter crushed with mortar and pestle, with the aim to turn the samples into a fine powder. This was very difficult to achieve, and some shreds of the plant material for each subsample did not turn into a powder.

Table 3. *The subsamples collected from the harvested biomass and the biomass belowground.*

Plant community	Subsamples of harvested biomass	Subsamples of belowground biomass
<i>Phragmites</i>	P1/5	PB1
	P7/1	PB2
	P9/5	PB3
	P13/1	PB4
	P19/2	PB5
<i>Typha</i>	T1/1	TB1
	T2/3	TB2
	T3/2	TB3
	T4/1	TB4
	T5/3	TB5

The final preparation for the C and N content analysis was performed at the iThemba Labs in Johannesburg. A fine balance was set to zero with a tin foil capsule between each sample preparation (Fig. 9). Five samples of each subsample were prepared by measuring 0.4-0.6 mg of biomass powder into a tin capsule. The capsule was thereafter folded into a ball about 3 mm in diameter with the use of forceps. It was important to remove all the air within the tin capsule during the folding. Each sample was stored in a marked well on a tray (Fig. 10). The mass and well location of each sample was noted. A total of 100 samples were prepared.

The prepared samples were thereafter analysed by the iThemba Labs on a Flash HT Plus Elemental Analyzer coupled to a Thermo Scientific Delta V Plus Isotope Ratio Mass Spectrometer by a ConFlo IV universal interface, supplied by Thermo Fisher (Thermo Fisher Scientific 2019-05-15). Laboratory standards and blanks were run after every 24 samples. C:N ratios were calculated by iThemba Labs from estimated mol of C respectively N in the samples, derived from the molecular masses of the elements in combination with the results from the C and N content analysis.

Mean C and N content and C:N ratio of each subsample were derived, along with community mean of C and N content and C:N ratio for *Phragmites* aboveground, *Typha* aboveground, *Phragmites* belowground and *Typha* belowground. Aboveground biomass in this context refers to the biomass harvested aboveground, and not the AG_{RF} (see section 3.2.1).



Figure 9. *Subsamples were prepared for analysis in tin capsules. Each capsule was folded into a ball with the use of forceps.*

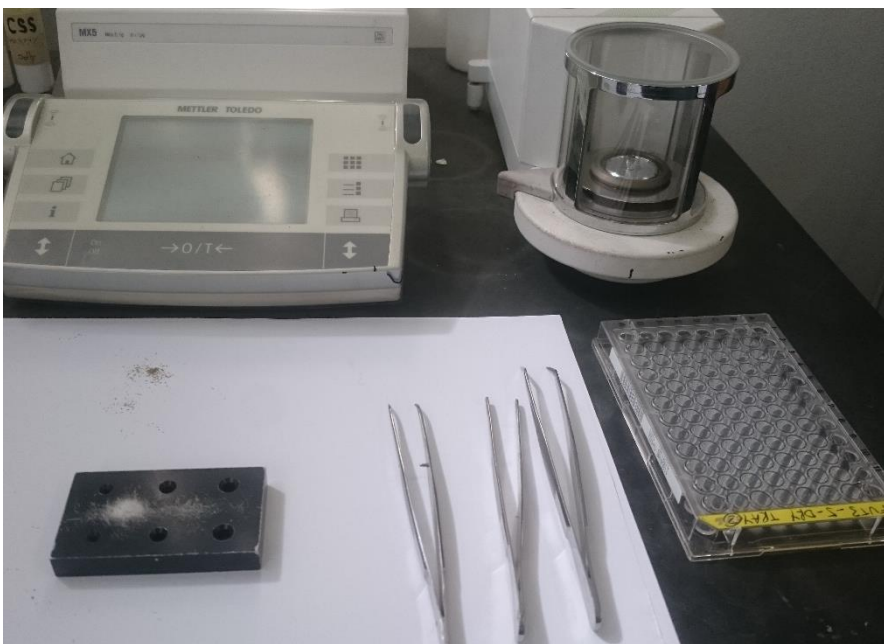


Figure 10. *In the upper part of the picture is the fine balance used for measuring the samples for the analysis. To the right in the picture is a tray with wells used for storing the samples collected in folded tin capsules.*

3.2.3 Estimating NPP

To estimate NPP, based on harvested biomass, the size of the Wakkerstroom wetland needed to be determined. A satellite image of the area captured on 2019.03.20 by Sentinel-2 with a resolution of 10 m was downloaded from EarthExplorer (Copernicus Sentinel Data 2019). Sentinel-2 is an imaging mission launched by Copernicus where two satellites, flying in the same orbit, produces high resolution images of the surface of the Earth in 13 spectral bands: four bands at 10 m, six bands at 20 m and three bands at 60 m spatial resolution (Sentinel 2019-04-18). The image was ingested into the software ArcMap. The red, green and blue spectral bands were combined with the ArcGIS Composite Bands tool to create a multiband raster and thus a colour image.

For calculating areas using polygons, ArcMap requires projected GIS data. The original Geographic Coordinate System WGS_1984 was therefore changed to the Projected Coordinate System WGS_1984_UTM_Zone_36S. To know the distribution of the plant communities in the wetland, an estimation of the area of each community was performed, creating polygons. Based on site observations and sampling locations, *Phragmites* was known to cover the majority of the wetland, and *Typha* was known to mainly be present on the edges of the wetland. The pink and light green parts of the wetland in the image were assumed to be *Phragmites*, while the darker green was *Typha* (Fig. 11). However, every area containing the dark green colour was not assumed to be *Typha* due to the presence of other wetland vegetation such as various sedge species. Once the polygons for each plant community were made, the areas were calculated. The whole area of the wetland was obtained by adding together the areas for the communities. The distribution of each plant community was calculated by dividing the community specific areas by the total area of the wetland.

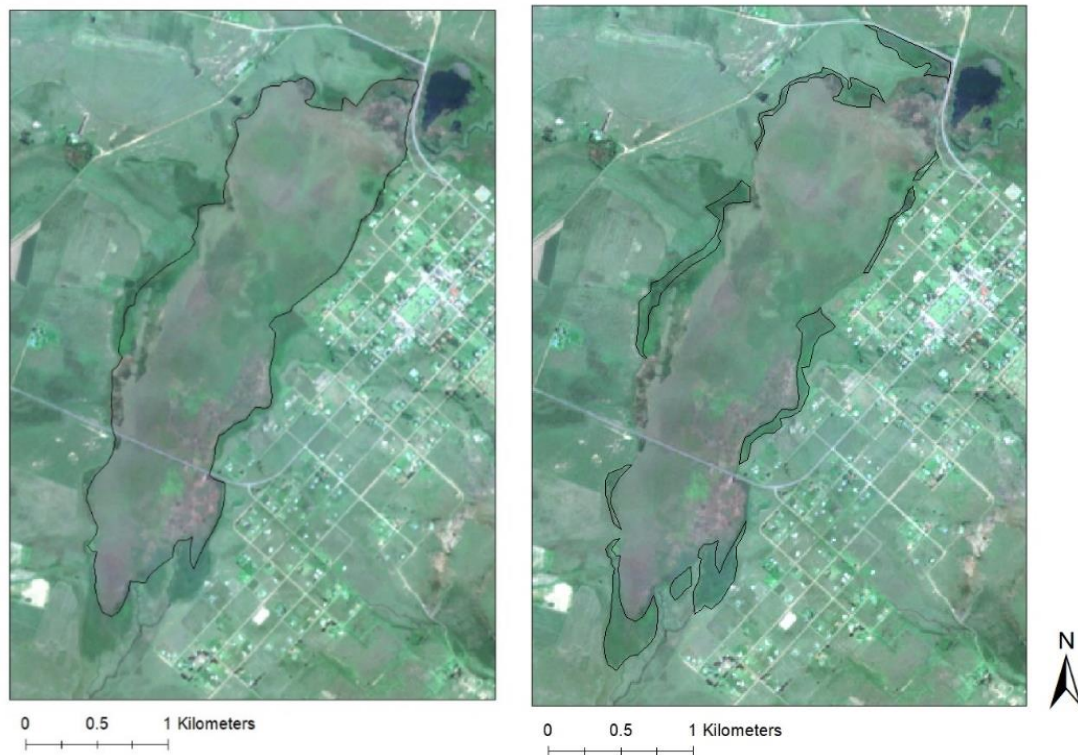


Figure 11. The polygons made for calculating the area of *Phragmites* (left) and *Typha* (right). © Copernicus Sentinel Data (2019).

A mean dry mass per area unit was calculated for *Phragmites* and *Typha*, based on the harvested material, using the community-specific mean DM content obtained in section 3.2.1. Since the biomass was harvested in quadrats of 0.25 m^2 , the mass was multiplied by four to obtain the mass of 1 m^2 . In accordance with Eq. 3, the area for each community, estimated from the Sentinel-2 image, was multiplied by the mean dry mass per area unit

to obtain the NPP_{AG} for the whole wetland. NPP_{AG} and the RF were used in Eq. 1 to calculate NPP_{tot} for each community. RF was calculated using Eq. 2, but due to the discovery of unusually low C content in the belowground material obtained from the C and N analysis (see section 4.1), mineral material was assumed to have adhered to the belowground biomass and contaminated the samples, thus was a mineral correction factor derived. The correction factor was obtained by assuming the same C content for the belowground material as for the aboveground biomass. The measured dry mass was assumed to contain both biomass and mineral material and a corrected dry mass for the belowground biomass was calculated. The dry mass of the AG_{RF} and corrected belowground biomass was used in Eq. 2 for calculating RF for each plant community. For more details about the RF calculations, see Tab. A5 in Appendix A. The NPP_{tot} for the whole wetland for both plant communities was obtained by adding together the NPP_{tot} for each community, resulting in the total NPP for the wetland for the growing season 2018/2019. NPP_{tot} for the growing season per area unit was derived by dividing NPP_{tot} with the estimated area of the wetland.

3.3 LUE MODELLING

3.3.1 FAPAR derived from MISR

In order to estimate NPP of the wetland using LUE modelling, pixels for deriving FAPAR within the wetland were needed. Eleven points, across the Wakkerstroom vlei, were used to find a suitable block and pixels for obtaining a record of FAPAR. Block 112 in path 168 covered the area of interest (Fig. 12).

Pixels of interest in the block were the ones containing the eleven points across the wetland. The resolution of each pixel was 275 x 275 m, and they were referred to as pixel number 1-11, beginning with the pixel in the north and ending with the one in the south (Fig. 13). The FAPAR values for each pixel were determined by the centre of the pixel. The distance between the centre of each pixel and the corresponding point can be seen in Tab. B3 in Appendix B.



Figure 12. Block 112 in path 168 covered the area of interest. © Google Earth (2019b).

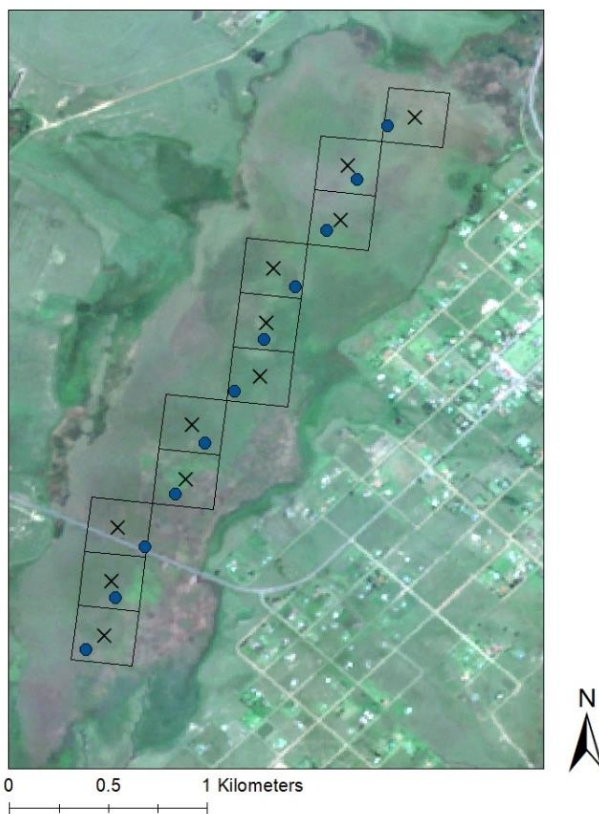


Figure 13. The eleven points (blue dots) covering the Wakkerstroom wetland were used to find suitable pixels for obtaining a record of FAPAR for the LUE modelling (Tab. B1, Appendix B). The eleven pixels in path 168 are shown as quadrats, along with the centre of the pixels marked with crosses. © Copernicus Sentinel Data (2019).

The TIP-product ABS_VIS (Absorptance factor in the visible spectrum), known as FAPAR, was extracted from pixels 1-11 for the time period 2000.03.24-2018.08.17 by the MISR team at the Global Change Institute at the University of the Witwatersrand. The record had been processed using the MISR-HR software version V2.00-0, and contained data derived with 16-day intervals.

Data displaying the value -9990 in the FAPAR record indicated a missing value, probably due to cloud coverage, and were thus removed. Since FAPAR was a scalar between 0-1, the few negative FAPAR values were incorrect and were thus removed from the record. The cost function produced by the MISR-HR, indicated the quality of the data. Cost values greater than 0.5 were suppressed by the software.

A record of daily FAPAR for each pixel was needed for the NPP calculation. Because of the 16-day intervals record and missing values due to cloud contamination and low-quality data, linear interpolation was used to fill the gaps in the daily record for each pixel (Eq. 15), where FAPAR data equals the y variable and the corresponding date equals the x variable.

$$y_{unknown} = y_1 + (x_{unknown} - x_1) \cdot \frac{y_2 - y_1}{x_2 - x_1} [-] \quad (15)$$

3.3.2 Calculating PAR

To calculate NPP with LUE modelling, daily values of Photosynthetically Active Radiation (PAR) were needed, which in turn required values of SW_{rad} . The final record of PAR was derived from SW_{rad} obtained from different sources (Tab. 4).

Table 4. Different sources of data were used for obtaining a record of SW_{rad} for the Wakkerstroom area between the years 2000-2018.

Time period	Type of record	Source
2000.02.01-2008.12.31	Monthly average of daily SW_{rad} .	Climatology data ^a for Wakkerstroom.
2009.01.01-2017.12.31	Monthly number of sunshine hours.	Obtained from World Weather Online (2019-04-26) for Volksrust ^b .
2018.01.01-2018.12.31	Average of hourly SW_{rad} .	Weather station located at the corner of Loop street and Van Der Schyff street in Wakkerstroom ^c .

^a See Tab. G1 in Appendix G for the climatology data.

^b See Fig. H2 in Appendix H for the location of Volksrust.

^c See Fig. H1 in Appendix H for the location of the weather station in Wakkerstroom.

The SW_{rad} used for the time period 2000.02.01-2008.12.31 was obtained from climatology data, derived from sunshine data recorded at weather stations at Standerton and Newcastle (Tab. G1, Appendix G) between the years 1960-1990, containing monthly average of daily SW_{rad} for the Wakkerstroom area.

A record of monthly number of sunshine hours was obtained for the time period 2009.01.01-2017.12.31 from World Weather Online (2019-04-26) for Volksrust (Tab. C1, Appendix C). The total number of sunshine hours per month was divided with the number of days for each month, resulting in the average hours of sunshine per day, which equals the parameter n in Eq. 6. The parameter N was calculated with Eq. 7, with ω obtained from Eq. 11 in combination with Eq. 9 and Eq. 10, where the latitude was set to -27.35° . To complete the calculations using Eq. 6, daily $SW_{rad,top}$ was derived from Eq. 8, using $I_{sc}=1367 \text{ W}\cdot\text{m}^{-2}$.

A record of hourly average of SW_{rad} for the time period 2018.01.01-2018.12.31 was obtained, measured at a weather station located at the corner of Loop street and Van Der Schyff street in Wakkerstroom. The record of SW_{rad} was measured in $\text{W}\cdot\text{m}^{-2}$, which equals $\text{J}\cdot\text{m}^{-2}\cdot\text{s}^{-1}$. The record was transformed to $\text{J}\cdot\text{m}^{-2}\cdot\text{day}^{-1}$ by multiplying the hourly SW_{rad} with the number of seconds per hour (3600 s), which equals $\text{J}\cdot\text{m}^{-2}\cdot\text{h}^{-1}$, and was then added together for each day to obtain $\text{J}\cdot\text{m}^{-2}\cdot\text{day}^{-1}$. The final record of average daily SW_{rad} for the years 2000-2018 was transformed to a record of daily PAR by using Eq. 5.

3.3.3 Conversion efficiency factor ϵ

In order to calculate NPP of the Wakkerstroom wetland using a LUE model, a conversion efficiency factor (ϵ) was needed, which was derived from the maximal value of the conversion efficiency (ϵ_{max}). ϵ_{max} varies for different types of vegetation, and no ϵ_{max} value specifically for wetland vegetation was found. It is important to separate C3 and C4 vegetation when estimating biomass productivity due to the higher Light Use Efficiency and higher photosynthetic efficiency of C4 compared to C3 vegetation (Liang et al 2012). Since the dominant plant communities in the Wakkerstroom vlei consist of C3 plants, an ϵ_{max} typical for C3 vegetation was assumed to be most appropriate. The values of ϵ_{max} used in previous studies were $1.43 \text{ g C}\cdot\text{MJ}^{-1}$ for soybeans, derived by Gitelson et al. (2015), and $1.8 \text{ g C}\cdot\text{MJ}^{-1}$, used by Yan et al. (2015) for C3 ecosystems. Based on these values, ϵ_{max} was estimated to be $1.6 \text{ g C}\cdot\text{MJ}^{-1}$ for this study.

The vegetation in the Wakkerstroom wetland was assumed to not suffer from water stress due to the permanently wet conditions, which implied that $f(W_s)$ in Eq. 12 was neglected. The attenuation function for the temperature, however, was required. The equation used for $f(T_s)$ was based on a non-linear hump-shaped Gompertz function (Eq. 16). This non-linear function was used instead of a linear function because of its ability to show “runaway” effects at high temperatures.

$$f(T_s) = \exp\left(\frac{c(1-T_s^d)}{d}\right) \cdot T_s^c \quad [-] \quad (16)$$

The function $f(T_s)$ consisted of the optimum temperature for vegetation growth (a), the lowest temperature where production stops (b), the slope below the optimum (c), and the slope above the optimum (d).

$$T_s = \frac{b - T_{\text{day}}}{b - a} \quad [-] \quad (17)$$

T_s was a function of daily temperature during daytime (T_{day}) (Eq. 17). The value of a was estimated as 27 °C for C3 vegetation and b was assumed to be 0 °C due to the occurrence of frost, which stops the vegetation growth (Scholes 2019³).

A calibration graph was used for customizing the slopes of the function, and c and d were determined by observing the behaviour of the calibration graph when changing the values. The calibration graph was made from $f(T_s)$, on the y-axis varying between 0-1, and the temperature interval 0-40 °C on the x-axis (Fig. D1, Appendix D). The slope below the optimum was aimed to accord with the temperature coefficient for biological systems, known as Q_{10} , which is the measurement of the rate of change of biological processes when increasing the temperature by 10 °C. Q_{10} for vegetation is around 2 (Tjoelker et al. 2001), and the value of c was determined based on this rate, which meant that the value of $f(T_s)$ should be doubled when increasing the temperature from 15 °C to 25 °C, resulting in the approximate value 2. The slope parameter d was estimated to be 6 from observing the calibration graph, where the aim was to find a steep downslope.

Due to the fact that there is no photosynthetic activity during night, an average temperature of the hours during daytime, T_{day} , was used. T_{day} was calculated using Eq. 18, where T_{mean} was the mean temperature, T_{max} was the maximum temperature and T_{min} was the minimum temperature of the day. See Fig. D2 in Appendix D for an example.

$$T_{\text{day}} = T_{\text{mean}} + 0.25(T_{\text{max}} - T_{\text{min}}) \quad [^{\circ}\text{C}] \quad (18)$$

Several temperature records from various sources were used to derive a record of T_{day} for calculating daily $f(T_s)$ (Tab. 5). A temperature record containing daily T_{min} , T_{max} and T_{mean} was used for calculating daily T_{day} for the time period 2000.02.01-2015.12.31. An hourly temperature record, measured at the Wakkerstroom weather station, was obtained for the time periods: 2016.01.01-2016.01.08, 2016.06.03-2016.12.31, 2017.01.01-2017.05.03 and 2018.01.01-2018.12.31. T_{min} , T_{max} and T_{mean} were determined for each day to calculate daily T_{day} . The hourly temperature record lacked data for the time periods 2016.01.09-2016.06.02 and 2017.05.04-2017.12.31. The gaps were filled with monthly T_{min} , T_{max} and T_{mean} from climatology data for the Wakkerstroom area.

The final record of daily T_{day} was used for calculating T_s with Eq. 17, which in turn was transformed to daily $f(T_s)$ with Eq. 16. Once the record of $f(T_s)$ was completed, daily ϵ was derived using Eq. 12 for the time period 2000.02.01-2018.12.31.

³ Personal communication 2019, Prof RJ Scholes, University of the Witwatersrand.

Table 5. Temperature records for calculating daily $f(T_s)$ was obtained from different sources.

Time period	Type of record	Source
2000.02.01-2015.12.31	Daily minimum, maximum and mean temperature.	Temperature record compiled by Moyo (2015), consisting of measurements obtained from weather station at Volksrust and patched with data from weather station at Wakkerstroom ^a .
2016.01.01-2016.01.08, 2016.06.03-2016.12.31, 2017.01.01-2017.05.03, 2018.01.01-2018.12.31	Average of hourly temperature.	Weather station located at the corner of Loop street and Van Der Schyff street in Wakkerstroom ^b .
2016.01.09-2016.06.02, 2017.05.04-2017.12.31	Monthly minimum, maximum and mean temperature.	Climatology data ^c for Wakkerstroom.

a See Fig. H2 in Appendix H for the locations of the weather stations.

b See Fig. H1 in Appendix H for the location of the weather station in Wakkerstroom.

c See Tab. G1 in Appendix G for the climatology data.

3.3.4 Calculating NPP

The final records of FAPAR, PAR and ϵ were compiled in Excel sheets. An Excel file was created for each of the eleven pixels covering the Wakkerstroom wetland and the sheets within each file were categorised by year (Fig. 14). The FAPAR records were pixel specific, while the records of PAR and ϵ were the same used for all pixels. GPP, calculated with Eq. 4, was used in Eq. 13 to obtain NPP. To calculate NPP_{tot} with Eq. 14, f_c was required. The mean C content of the harvested samples of *Phragmites* and *Typha*, described in section 3.2.2, were around 44 % for both plant communities (Tab. 6), and f_c was therefore set to 0.44. By using one f_c value instead of two, no separation of the NPP_{tot} calculations regarding the different communities were needed, which made the calculations easier to perform.

	A	C	D	E	F	G	H	I	J	K	L	
1	Calculation of NPP for the Wakkerstroom wetland between 2000-2018 for pixel 1.								fc=	0.44		
2												
3	Date	FAPAR	PAR	e	GPP	NPP	NPPtot					
4		-	MJ/m2*day	g C/MJ	g C/m2*day	g C/m2*day	g/m2*day					
5	2001-01-01	0.580	5.3505	1.188503	3.687038497	1.843519249	4.18981647					
6	2001-01-02	0.585	5.3505	0.38358	1.201349475	0.600674738	1.36516986					
7	2001-01-03	0.591	5.3505	0.549286	1.736636834	0.868318417	1.97345095					
8	2001-01-04	0.596	5.3505	0.852717	2.721287566	1.360643783	3.09237223					
9	2001-01-05	0.602	5.3505	1.188503	3.828169157	1.914084579	4.35019222					
10	2001-01-06	0.602	5.3505	1.516537	4.884765846	2.442382923	5.55087028					
11	2001-01-07	0.598	5.3505	1.171666	3.751691295	1.875845647	4.26328556					
12	2001-01-08	0.595	5.3505	1.333864	4.245727505	2.122863753	4.82469035					
13	2001-01-09	0.591	5.3505	1.557298	4.927360273	2.463680137	5.59927304					
14	2001-01-10	0.588	5.3505	1.599967	5.031990122	2.515995061	5.71817059					
15	2001-01-11	0.584	5.3505	1.556205	4.864810934	2.432405467	5.52819424					
16	2001-01-12	0.581	5.3505	1.598175	4.965667681	2.48283384	5.64280418					
17	2001-01-13	0.577	5.3505	1.519416	4.692112197	2.346056099	5.33194568					
18	2001-01-14	0.574	5.3505	1.5646	4.801939415	2.400969707	5.45674934					
19	2001-01-15	0.570	5.3505	0.864643	2.637273622	1.318636811	2.99690184					
20	2001-01-16	0.567	5.3505	1.437949	4.358632123	2.179316061	4.95299105					
21	2001-01-17	0.563	5.3505	1.202857	3.623195266	1.811597633	4.11726735					
22	2001-01-18	0.559	5.3505	1.472079	4.406187719	2.203093859	5.0070315					
23	2001-01-19	0.556	5.3505	1.522176	4.558852281	2.278976146	5.10176287					
	...	2008	2007	2006	2005	2004	2003	2002	2001	2000	NPP growing season	+

Figure 14. The final record of FAPAR, PAR and ϵ were compiled in Excel sheets, categorised by years, for calculating GPP, NPP and NPP_{tot}. One Excel file was created for each of the eleven pixels covering the Wakkerstroom wetland. The Excel file in the figure represents pixel 1.

Since it was desirable to investigate annual NPP of the wetland, annual NPP_{tot} for the years 2000-2018 was calculated by adding together daily NPP_{tot} for the period 1st of July-30th of June, which was referred to as a growing season. The actual growing season in this part of South Africa generally occurs between September and April (Vrieling et al. 2013) and not all year. The phenology of FAPAR reflects the growing season, so by adding together the daily NPP_{tot} for an entire year the production of the growing season was included in that time period. The growing seasons were referred to as the years when the season started and ended, e.g. 2003/2004 equals the growing period 2003.07.01-2004.06.30. This means that the growing seasons included 365 days for normal years and 366 days for leap years. A record of mean NPP_{tot} for the whole wetland for each growing season was derived from the NPP_{tot} from each pixel. To obtain a record of NPP_{tot} for the whole Wakkerstroom vlei for the growing seasons, the annual record of mean NPP_{tot} were multiplied by the area of the wetland, estimated from the Sentinel-2 image described in section 3.2.3.

3.4 METHOD COMPARISON OF NPP, AND CALCULATION OF NITROGEN UPTAKE

As a first step, the NPP_{tot} estimated from harvested biomass (NPP_{harvest}) was compared to the NPP_{tot} derived from LUE modelling (NPP_{LUE}), with standard deviations of NPP_{LUE} as error bars. As a second step, the record of mean NPP_{LUE} and community mean N

content obtained from the harvested biomass aboveground were used to determine the nitrogen uptake of the Wakkerstroom vlei. The amount of biomass produced by the *Phragmites* community and the *Typha* community for each growing season were calculated respectively by multiplying the mean NPP_{tot} for the whole wetland with the distribution of each plant community, estimated from the Sentinel-2 image in section 3.2.3 (Eq. 19). The annual production of each community was multiplied by the community specific mean N content (Eq. 20).

$$NPP_{Community} = NPP_{tot} \cdot \text{distribution} [\text{kg}\cdot\text{m}^{-2}\cdot\text{season}^{-1}] \quad (19)$$

$$N \text{ uptake}_{Community} = NPP_{Community} \cdot N \text{ content}_{Community} [\text{kg}\cdot\text{m}^{-2}\cdot\text{season}^{-1}] \quad (20)$$

The sum of the nitrogen uptake of each community resulted in the annual nitrogen uptake of the whole wetland for each growing season. By dividing the record with the estimated area of the wetland, the mean nitrogen uptake per area unit was obtained.

4. RESULTS

4.1 CARBON AND NITROGEN CONTENT IN THE WETLAND VEGETATION

The community mean of material harvested belowground did not correspond to spatial variance since the samples used for deriving the subsamples were mixed together in the same paper bag. The mean C:N ratio for each community had generally a high analytical standard deviation, due to variance in both the C and N estimate (Tab. 6). See Fig. F1 in Appendix F for the complete result of the analysis.

Table 6. Mean, standard deviation and community mean of the C and N content and the C:N ratio of the dried subsamples analysed at the iThemba Labs. The standard deviation for each subsample corresponds to the analytical variance, obtained from five analysed samples per subsample. The standard deviation for the community means aboveground (AG) represents the spatial variance. No spatial variance exists for the biomass sampled belowground (BG) due to mixing of samples. The C:N ratio was based on the mol ratio of C and N for each sample.

Plant community	Subsample	Location	C [%]	N [%]	C:N ratio [-]
<i>Phragmites</i> , AG	P1/5	1	44.3 ± 1.14	2.10 ± 0.11	24.7 ± 0.88
	P7/1	5	43.8 ± 0.49	0.82 ± 0.05	62.5 ± 3.78
	P9/5	6	44.3 ± 0.95	1.05 ± 0.20	50.8 ± 10.0
	P13/1	7	42.9 ± 1.47	1.92 ± 0.31	26.7 ± 4.93
	P19/2	9	43.7 ± 0.49	0.58 ± 0.04	88.7 ± 6.23
Community mean			43.8 ± 1.03	1.29 ± 0.64	50.7 ± 24.9
<i>Typha</i> , AG	T1/1	1	44.0 ± 0.26	1.39 ± 0.13	31.2 ± 3.45
	T2/3	2	44.8 ± 0.32	1.34 ± 0.06	39.2 ± 1.67
	T3/2	3	44.4 ± 0.31	0.53 ± 0.06	99.0 ± 10.1
	T4/1	3	45.2 ± 2.83	0.67 ± 0.13	80.6 ± 11.6
	T5/3	1	42.2 ± 0.48	1.10 ± 0.20	46.2 ± 8.34

Community mean			44.2 ± 1.60	1.00 ± 0.37	60.4 ± 26.4
<i>Phragmites</i> , BG	PB1	1	23.5 ± 2.75	0.76 ± 0.04	36.0 ± 3.37
	PB2	1	22.2 ± 2.41	0.54 ± 0.03	48.0 ± 4.49
	PB3	1	20.0 ± 2.53	0.56 ± 0.02	41.2 ± 4.47
	PB4	1	16.4 ± 2.12	0.51 ± 0.03	37.5 ± 3.21
	PB5	1	11.0 ± 0.94	0.49 ± 0.02	26.4 ± 1.68
Community mean			18.6 ± 5.01	0.57 ± 0.10	37.8 ± 7.92
<i>Typha</i> , BG	TB1	1	37.1 ± 0.44	0.90 ± 0.03	48.0 ± 1.78
	TB2	1	36.1 ± 0.71	0.75 ± 0.06	56.3 ± 5.12
	TB3	1	37.7 ± 0.53	0.45 ± 0.02	97.1 ± 3.97
	TB4	1	36.9 ± 0.23	0.74 ± 0.02	58.5 ± 1.65
	TB5	1	36.8 ± 0.82	0.68 ± 0.03	63.5 ± 1.74
Community mean			36.9 ± 0.74	0.70 ± 0.15	64.7 ± 17.6

4.2 NPP

4.2.1 NPP based on harvested biomass

The estimated NPP was calculated from biomass harvested aboveground, converted to dry mass using community specific mean dry matter (DM) content. The mean DM content for the *Phragmites* community was 0.39 and 0.26 for the *Typha* community (Tab. 7). Community specific root fractions (RF) were needed for the NPP calculations obtained from dry mass of harvested belowground and aboveground material (Tab. A4, Appendix A). A mineral correction factor was applied for calculating a corrected dry mass of the belowground material, due to the inferred sediment contamination of the samples. RF was estimated to be 0.23 for the *Phragmites* community and 0.61 for the *Typha* community (Tab. 8).

Table 7. Mean dry matter (DM) content in wet mass of *Phragmites* and *Typha*, calculated from total wet mass and total dry mass of aboveground (AG) biomass, dried in a drying oven.

Plant community	Total wet mass [g]	Total dry mass [g]	Mean DM content [-]
<i>Phragmites</i> , AG	4646.0	1827.6	0.39
<i>Typha</i> , AG	4606.5	1188.6	0.26

Table 8. The root fraction (RF) calculated from the total dry mass of aboveground (AG_{RF}) and belowground (BG) biomass, corrected with a mineral correction factor. The dry mass of AG_{RF} was obtained using the community specific DM content (Tab. 7).

Plant community	Total dry mass, AG_{RF} * [g]	Total dry mass, BG [g]	Mineral correction factor [-]	Corrected dry mass, BG [g]	RF [-]
<i>Phragmites</i>	197.5	135.3	0.425	57.5	0.23
<i>Typha</i>	133.5	248.8	0.835	207.7	0.61

* Calculated with mean DM content in Tab. 7.

The total NPP representing aboveground and belowground biomass (NPP_{tot}), calculated from aboveground NPP (NPP_{AG}), root fraction and area of the wetland, was estimated to $2.01 \text{ kg}\cdot\text{m}^{-2}$ for the growing season 2018/2019. The NPP_{tot} for the whole permanently wet part of the Wakkerstroom vlei (416 ha) was estimated to 8353 megagrams (Mg) dry mass, where *Phragmites* was estimated to produce 6123 (73 %) Mg of biomass and *Typha* 2230 (27 %) Mg (Tab. 9).

Table 9. Estimated NPP for aboveground material (NPP_{AG}) expressed in megagrams (Mg) was calculated from dry mass per area unit (\bar{m}) of the harvested biomass and estimated area of each community, representing the growing season 2018/2019. NPP_{AG} was converted to total NPP (NPP_{tot}) for the whole Wakkerstroom vlei using root fraction (RF). NPP_{tot} per area unit was obtained by dividing the NPP_{tot} for the whole Wakkerstroom vlei with the total area of the wetland.

Plant community	\bar{m} [$\text{kg}\cdot\text{m}^{-2}\cdot\text{season}^{-1}$]	Area [m^2]	Distribution [%]	NPP_{AG} * [$\text{Mg}\cdot\text{season}^{-1}$]	RF [-]	NPP_{tot} * [$\text{Mg}\cdot\text{season}^{-1}$]	NPP_{tot} [$\text{kg}\cdot\text{m}^{-2}\cdot\text{season}^{-1}$]
<i>Phragmites</i>	1.33 ± 0.516	3537351	85	4715	0.23	6123	1.73
<i>Typha</i>	1.41 ± 0.562	617713	15	870	0.61	2230	3.61
Total	-	4155064	100	-	-	8353	2.01

* For the whole Wakkerstroom vlei.

4.2.2 NPP based on LUE modelling

Mean NPP_{tot} per area unit, obtained from LUE modelling, varied between $0.49\text{-}1.64 \text{ kg}\cdot\text{m}^{-2}$, with an average of $1.04 \text{ kg}\cdot\text{m}^{-2}$ for the growing seasons between 2000-2018. The whole wetland was estimated to produce between 2033-6818 Mg with an average of 4332 Mg (Tab. 10) and an 18-year standard error of 10 %. The growing seasons referred to the period 1 July-30 June, meaning that NPP for the growing seasons included 365 days for normal years and 366 days for leap years.

Table 10. Mean, standard deviation and average of NPP_{tot} in kg per area unit per growing season and NPP_{tot} for the whole Wakkerstroom vlei (416 ha) in megagrams (Mg) per growing season, obtained from LUE modelling.

Growing season	Mean NPP_{tot}	Mean NPP_{tot} *
	[$kg \cdot m^{-2} \cdot season^{-1}$]	[$Mg \cdot season^{-1}$]
2000/2001	0.62 ± 0.01	2554 ± 52
2001/2002	0.64 ± 0.01	2663 ± 51
2002/2003	0.65 ± 0.02	2709 ± 75
2003/2004	0.68 ± 0.01	2811 ± 26
2004/2005	0.68 ± 0.00	2823 ± 16
2005/2006	0.63 ± 0.09	2607 ± 391
2006/2007	0.70 ± 0.12	2913 ± 440
2007/2008	0.49 ± 0.01	2033 ± 55
2008/2009	1.09 ± 0.01	4531 ± 45
2009/2010	1.34 ± 0.03	5552 ± 103
2010/2011	1.53 ± 0.06	6373 ± 237
2011/2012	1.62 ± 0.05	6740 ± 186
2012/2013	1.53 ± 0.02	6343 ± 79
2013/2014	1.48 ± 0.05	6157 ± 216
2014/2015	1.05 ± 0.15	4369 ± 612
2015/2016	1.17 ± 0.1	4863 ± 410
2016/2017	1.64 ± 0.07	6818 ± 275
2017/2018	1.23 ± 0.01	5120 ± 58
Average	1.04 ± 0.41	4332 ± 1705

* For the whole Wakkerstroom vlei.

4.2.3 Comparison of NPP from harvested biomass and NPP from LUE modelling

The NPP_{tot} calculated from LUE modelling (NPP_{LUE}) per area unit for the growing seasons between 2000-2018 were lower compared to the NPP_{tot} estimated from biomass harvested in the end of the growing season 2018/2019 ($NPP_{harvest}$) (Fig. 15). $NPP_{harvest}$ ($2.01 kg \cdot m^{-2}$) was approximately four times higher compared to the lowest NPP_{LUE} value ($0.49 kg \cdot m^{-2}$), and 1.2 times higher than the highest NPP_{LUE} value ($1.64 kg \cdot m^{-2}$), with the standard error of $\pm 0.04 kg \cdot m^{-2}$ for NPP_{LUE} .

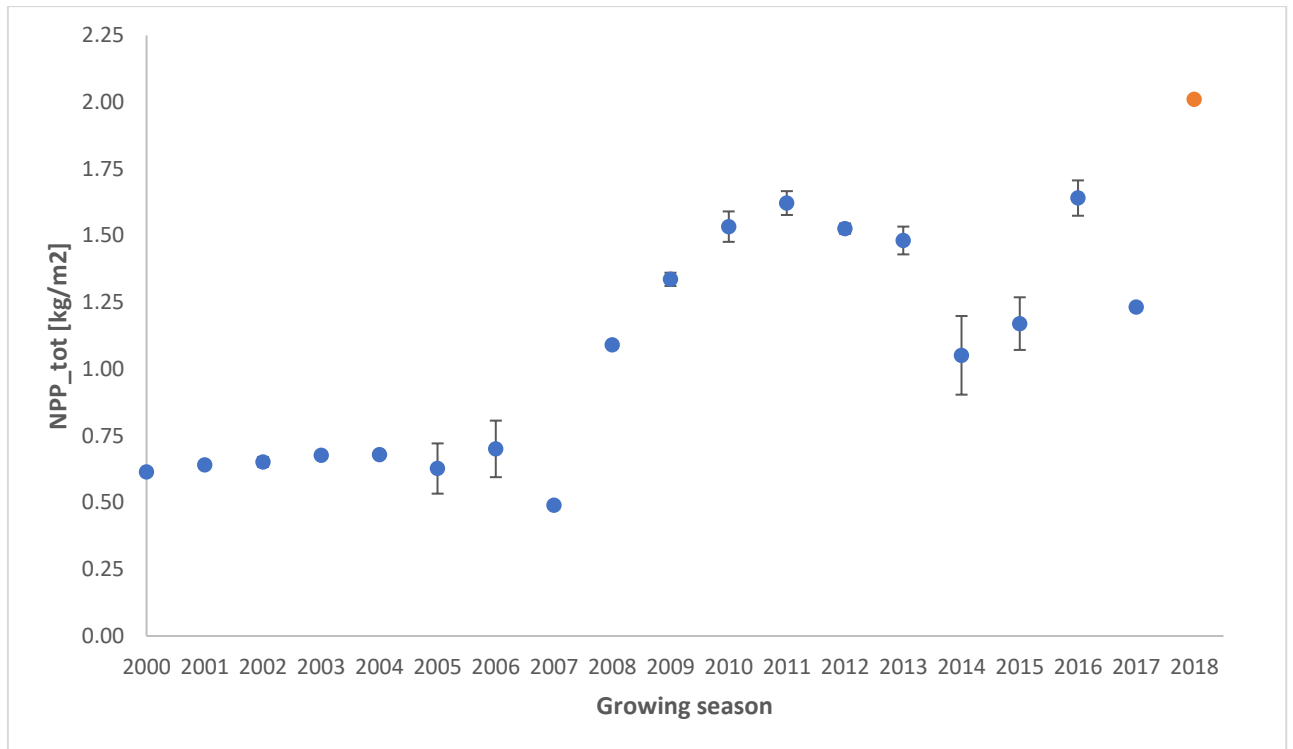


Figure 15. Mean NPP_{tot} calculated from LUE modelling (blue) per area unit for the growing seasons between the years 2000-2018 with standard deviations, compared to the NPP_{tot} estimated from biomass harvest in the end of the growing season 2018/2019 (orange). The growing seasons in the figure are referred to as the year when the season was initiated, e.g. 2000 represents the growing season 2000/2001.

4.3 NITROGEN UPTAKE OF THE WETLAND VEGETATION

The nitrogen uptake of the Wakkerstroom vlei was estimated from NPP_{tot} for the growing seasons between 2000-2018 of the wetland (Tab. 10), and the N content found in the harvested biomass (Tab. 6). The annual nitrogen uptake of the vegetation in the Wakkerstroom vlei was estimated to vary between 25.4-85.0 Mg nitrogen for the growing seasons between 2000-2018. The nitrogen uptake per area unit varied between 6.10-20.5 g N·m⁻² per growing season.

Table 11. Mean and average of nitrogen (N) uptake by the *Phragmites* community and the *Typha* community, respectively, for the whole Wakkerstroom vlei during the growing seasons between the years 2000-2018 displayed in megagrams (Mg), along with the N uptake per area unit.

Growing season	NPP_{tot}, <i>Phragmites</i> [Mg ·season⁻¹]	NPP_{tot}, <i>Typha</i> [Mg ·season⁻¹]	N uptake, <i>Phragmites</i> [Mg N ·season⁻¹]	N uptake, <i>Typha</i> [Mg N ·season⁻¹]	Total N uptake [Mg N ·season⁻¹]	Total N uptake per area unit [g N·m⁻² ·season⁻¹]
2000/2001	2171	383	28.0	3.83	31.8	7.66
2001/2002	2264	399	29.2	3.99	33.2	7.99
2002/2003	2303	406	29.7	4.06	33.8	8.13
2003/2004	2389	422	30.8	4.22	35.0	8.43
2004/2005	2400	423	31.0	4.23	35.2	8.47
2005/2006	52216	391	28.6	3.91	32.5	7.82
2006/2007	2476	437	31.9	4.37	36.3	8.74
2007/2008	1728	305	22.3	3.05	25.4	6.10
2008/2009	3851	680	49.7	6.80	56.5	13.6
2009/2010	4719	833	60.9	8.33	69.2	16.7
2010/2011	5417	956	69.9	9.56	79.4	19.1
2011/2012	5729	1011	73.9	10.1	84.0	20.2
2012/2013	5391	951	69.6	9.51	79.1	19.0
2013/2014	5233	924	67.5	9.24	76.8	18.5
2014/2015	3714	655	47.9	6.55	54.5	13.1
2015/2016	4134	729	53.3	7.29	60.6	14.6
2016/2017	5795	1023	74.8	10.2	85.0	20.5
2017/2018	4352	768	56.1	7.68	63.8	15.4
Average	3682	650	47.5	6.50	54.0	13.0

5. DISCUSSION

5.1 NPP

5.1.1 NPP estimated from harvested biomass

According to Mitsch and Gosselink (2015), NPP in wetlands usually varies between 0.4-2 kg·m⁻² per year depending on the wetland type. The NPP_{tot} estimated in this study from harvested biomass in the end of the growing season 2018/2019 resulted in 2.01 kg·m⁻², meaning that the Wakkerstroom vlei belongs to the more productive wetlands. This value may be an overestimate, since the aim was to sample first-year growth at sites where a fire had occurred the previous growing season, in some cases carry-over from the previous season's production may have been inadvertently included. The *Phragmites* community was estimated to produce 1.73 kg·m⁻² and the *Typha* community 3.61 kg·m⁻² per growing season (Tab. 9). Meuleman et al. (2002) estimated one-year production of *Phragmites australis* to be 3.23 kg·m⁻² in a natural wetland and 6.99 kg·m⁻² in a constructed wetland used for wastewater treatment, both located in the Netherlands. This was quite surprising since the production obtained from harvested biomass in the Wakkerstroom wetland was lower compared to the production obtained by Meuleman et al. (2002), whereas it is usually assumed that near-tropical wetlands would produce more than temperate wetlands. However, the Wakkerstroom location is at high altitude, with a relatively cool climate, with no production for about half of the year due to frost. The comparison does give an indication that the results of the Wakkerstroom study are reasonable.

Improvements for future studies of NPP by harvesting biomass in the Wakkerstroom wetland, would be to sample biomass only on sites burned in the previous winter season; or to measure the standing biomass at the beginning of the growing season as well as at the end. The shortage of oven-drying space in this study meant that only a subset of samples was dried, and a dry matter content calculated; this dry matter content was then used to correct the wet mass, as weighed immediately after harvest, to an estimated dry mass. It would be better to dry all the harvested biomass before weighing, to avoid potential errors due to fluctuating moisture content.

To avoid underestimation of the total biomass production, the root fraction should also be harvested as accurately as possible. If the belowground material is too difficult to sample, an estimation of the root fraction, similar to the one conducted in this study, can be performed. This can be checked against root fraction values found in literature for the sampled species. It is desirable to rinse the belowground material thoroughly to avoid contamination by mud; but the risk is losing fine roots in the process. Therefore, a gentle wash followed by an ash-content correction is probably more accurate. It is also a possibility that some small area-error occurred as a result of misclassifying plant communities on the relatively-course resolution (10 m) satellite image used. This could be improved by using a finer resolution image.

5.1.2 NPP calculated from LUE modelling

The NPP_{tot} calculated from LUE modelling (NPP_{LUE}) has increased in the Wakkerstroom wetland over the period of satellite observations, 2000-2018 (Fig. 15). An interesting step change in NPP_{LUE} appeared to occur between the growing seasons 2007/2008 and 2008/2009. One possible reason behind this abrupt change is the installation of the sewage disposal system, which took place approximately 10 years ago. Paradoxically, this was probably when major wastewater contamination began, since the reticulated wastewater system never functioned properly, and leaked directly into the wetland. Prior to this, wastewater was accumulated in “conservancy tanks” on each property in the town, and was pumped out periodically by a sewage tanker for disposal at a site some distance from the wetland. The wastewater leakage could have resulted in the alleviation of nitrogen limitation in the wetland vegetation. In presence of increased availability of nutrients, the productivity of wetland vegetation generally increases (Kadlec and Wallace 2009), thus generating a higher NPP compared to previous growing seasons.

A second explanation for the increase of NPP_{LUE} is a change in climate. An increase of the average temperature can affect vegetation in parts of Africa in a negative way due to increased transpiration, leading to water stress. Although the night-time minimum and daytime maximum temperatures have risen by 2.3 and 0.9 °C respectively since 1910 at this location (Moyo 2015), there was no sudden increase between 2008 and 2009. Rainfall has also decreased by about 10 % over this period, but due to the permanently wet conditions in the Wakkerstroom wetland, the vegetation does not suffer from water stress in a great extent.

Another possibility for the drastic increase of NPP_{LUE} is the change in data feeding the LUE model. Both PAR and ϵ were computed with data obtained from different sources. PAR was derived from climatology data containing monthly average of daily SW_{rad} , derived from sunshine data measured at Standerton and Newcastle, between 2000-2008. Monthly number of sunshine hours for Volksrust were used for deriving PAR between 2009-2017 (Tab. 4). They represent different approaches for obtaining PAR, which might have different effects on the final NPP. The sampling locations could also have caused variations between the data sets since Volksrust is closer to Wakkerstroom compared to Standerton and Newcastle (Fig. H2, Appendix H). The temperature record for computing ϵ between 2000-2015 consisted of data measured at Volksrust and patched where necessary with data from Wakkerstroom. A temperature record measured at Wakkerstroom was used for the remaining time period, gap-filled with climatology data for periods lacking measurements (Tab. 5). Wakkerstroom and Volksrust are approximately 30 km apart, and at the same altitude. A previous study (Moyo 2015) showed no difference between their average temperature, for periods where data was available for both. Nonetheless, since the records were obtained in different ways and measured at different sampling locations, the possibility of error must be considered.

The LUE model created for this study is quite simple, but it provides an efficient way for quantifying primary production of terrestrial ecosystems. It is a linear product of four terms: FAPAR, PAR, $f(T_s)$ and ϵ_{max} . The reliability of the model depends directly on the reliability of the input data; the uncertainty in the final GPP is proportionally affected by errors in any of the terms. The record of FAPAR was derived from a block in one path,

providing FAPAR with 16-day intervals. Some values were missing due to cloud contamination, and gaps were filled with interpolated values. The gaps between missing values occasionally extended for several weeks, thus missing information about that period of time. It is possible to obtain a denser FAPAR record by using several paths, as long as they overlap the area of interest. The MISR-team at the University of the Witwatersrand had only processed FAPAR from one path at the time of this study. Using an extended FAPAR record derived from several paths is recommended for future LUE modelling of the Wakkerstroom area; but this is unlikely to have a dramatic effect on the results, since the 18-year dataset was already quite rich for this type of study (on average, more than 230 valid datapoints).

A reliable record of SW_{rad} is of importance when computing GPP. PAR (400-700 nm) was calculated as a constant fraction of SW_{rad} (300-3000 nm) in accordance with Eq. 5, the standard expression used in models simulating terrestrial production (Liang et al. 2012). Yuan et al. (2014) discovered that LUE models, similar to the one used in this study, tend to underestimate NPP for cloudy days, presumably because they did not sufficiently account for diffuse radiation. The same effect might have occurred for the data fed to this study's LUE model. Actual SW_{rad} observations were only available for 2018 (Tab. 4) from a newly-established weather station a few hundred metres from the wetland. Monthly averages of daily SW_{rad} were estimated from climatology data for the period 2000-2008, based on sunshine data recorded at weather stations at Standerton and Newcastle (Tab. G1, Appendix G), approximately 80 km northwest and 50 km south of Wakkerstroom respectively. Monthly number of sunshine hours for Volksrust was used for 2009-2017. The SW_{rad} record from the climatology data was computed in a similar manner as the SW_{rad} calculated from monthly sunshine hours (see Eq. 6-11). However, the record from the climatology data was based on sunshine data between 1960-1990, which does not necessarily represent the present monthly average of daily SW_{rad} . In future, the actual SW_{rad} recorded at Wakkerstroom should be used.

The greatest source of bias is probably due to the conversion efficiency factor (ϵ). The ϵ_{max} value used in this study was based on values for C3 vegetation obtained from two different studies. A larger set of specifically wetland-derived (preferably *Phragmites* and *Typha* communities) values of ϵ_{max} would be desirable, to allow the uncertainty in this number to be assessed.

The function used for the temperature modification factor $f(T_s)$ was a non-linear, hump-shaped Gompertz function. This was preferable to the usual practice of applying a monotonically-increasing exponential function (such as Q_{10}) since the latter overestimates on hot days. Another function used for $f(T_s)$ in LUE modelling is a linear function, usually referred to as T_{scalar} (Nuarsa et al. 2018). Since T_{scalar} does not account for the suppression of growth effects at high temperatures due to elevated respiration, it also tends to overestimate $f(T_s)$ above the temperature optimum, and also at low temperatures due to its linear assumptions. To evaluate the potential biases caused by choice of $f(T_s)$, a series of sensitivity analysis using different formulations could be performed.

5.1.3 Comparison of the two methods for obtaining NPP

NPP_{tot} based on the harvested material ($NPP_{harvest}$) was estimated in this study to be higher than the NPP_{LUE} (Fig. 15). Since no NPP_{LUE} for the growing season 2018/2019 could be obtained (the FAPAR product only extended to August 2018), a direct comparison of the $NPP_{harvest}$ and NPP_{LUE} could not be performed. Both methods have well-documented faults, thus it is difficult to tell which method is the more accurate one. One explanation of the different results is that $NPP_{harvest}$ was overestimated due to the harvest of more than one-year production. The root fraction used for computing $NPP_{harvest}$ might have been incorrect due to inadequate sampling and contamination by mineral material. Another explanation is the assumption that NPP equals 50 % of GPP (Eq. 13), the other half is lost due to respiration. This assumption, which has no theoretical basis, is widely made in simple LUE models (Chapin et al. 2011; Liang et al. 2012). The alternative is to explicitly model respiration, but that requires a large number of other parameters to be determined. NPP_{LUE} was calculated using C fraction (Eq. 14) obtained in the harvested biomass, which was estimated to 44 %. The C content may vary somewhat between years, but not much. The assumption that plant dry matter is approximately 50 % C (Chapin et al. 2011) is widely made.

The theory behind using remotely sensed data for estimating GPP, described in section 2.2.2, is based on the assumption that NPP is related to the amount of solar energy absorbed by the vegetation. PAR directly affects vegetation growth by controlling carbon exchange between the atmosphere and plant canopy (Gitelson et al. 2015). The second assumption of the theory states that there is a relation between vegetation indices derived from satellites and absorbed solar energy. FAPAR is solar radiation absorbed by green vegetation (Liang et al. 2012) and could in theory be “misderived” for non-green or semi-green vegetation. It should also be possible to miss out vegetation due to shading, but since LUE modelling mainly is used for estimating production in global scale, neglecting small quantities of biomass does not have a big impact on the overall result. Typically, FAPAR is derived from leaf area index (LAI) and is thus dependent on the surface of the vegetation absorbing radiation (Coops et al. 2010). This statement implies that FAPAR is determined by the direction of the sensor in relation to the vegetative surface. This is not an entirely fair assumption since most of the plant surfaces are not orthogonal in relation to the sensors, meaning that a major part of the vegetation is not fully captured by the instrument. The FAPAR from the MISR-instrument has the advantage of obtaining a highly-calibrated spectral reflectance from nine directions, thus deriving more accurate products compared to similar satellite sensors (Verstraete et al. 2012).

The theoretical value of ϵ can be derived from the quantum efficiency of photosynthesis, integrated over the whole canopy and over time. However, according to assumption 3), ϵ is lower than the optimum (ϵ_{max}) due to biophysical reasons such as low temperatures and water stress. The value of ϵ_{max} selected has a direct impact on the calculated NPP. For this study, ϵ_{max} was unknown and had to be estimated based on values typical for C3 vegetation. It would be preferable to have an ϵ_{max} specifically for wetland ecosystems, along with an uncertainty estimate. A too-low value of ϵ_{max} might have led to underestimation of the production of the Wakkerstroom wetland using the LUE approach.

5.2 CARBON AND NITROGEN CONTENT IN THE WETLAND VEGETATION

The spatial variability of N content for the aboveground *Phragmites* community (± 0.64 %) and *Typha* community (± 0.37 %), obtained from the C and N content analysis (Tab. 6), could be due to the inflow of nitrogen rich wastewater at the upper end of the wetland, causing various concentrations of nitrogen in the wetland. When comparing the mean N content found in the subsamples of *Phragmites*, P1/5 contained the highest value (2.10 ± 0.11 %) followed by P13/1 (1.92 ± 0.31 %). P1/5 represents location 1 (Fig. 4), close to the point at which the Wakkerstroom river enters the wetland and thus one of the first places to be exposed to wastewater. P13/1 was harvested at location 7, situated at the distant edge of the wetland, close to location 9 where P19/2 (0.58 ± 0.04 %) was sampled. P9/5, harvested at location 6, had a higher N content (1.05 ± 0.20 %) compared to P7/1 (0.82 ± 0.05 %) from location 5, which is closer to the sewage nitrogen source. The *Typha* communities were sampled at three locations at the northern end of the wetland, close to one another. It is therefore difficult to distinguish differences in N content in relation to distance to the Wakkerstroom river. The subsamples T3/2 (0.53 ± 0.06 %) and T4/1 (0.67 ± 0.13 %), both harvested at location 3, contained the lowest N content of the *Typha* subsamples. This might be due to less exposure of wastewater for that particular part of the wetland, which is unlikely as the location is situated close to the main water inflow, as are location 1 and 2, where the other subsamples of *Typha* originates from. Based on these observations, no specific pattern is shown between N content in the harvested biomass and distance to the inlet point of the wastewater in the wetland.

Vymazal and Kröpfelová (2010) reported N content found in *Phragmites australis* to be in the range $12.7\text{-}23.6 \text{ g N}\cdot\text{kg}^{-1}$ ($1.27\text{-}2.36$ %) for dry mass aboveground, and between $13.3\text{-}19.8 \text{ g N}\cdot\text{kg}^{-1}$ ($1.33\text{-}1.98$ %) for dry mass belowground, sampled in two constructed wetlands in the Czech Republic. The community mean N content found in this study for the *Phragmites* community was 1.29 % for dry biomass harvested aboveground, and 0.57 % for dry mass belowground (Tab. 6). The comparison of Wakkerstroom to the Czech Republic is not entirely valid, due to the differences in environmental conditions between the two sites. Organic nitrogen generally makes up 1-7 % of the dry mass of the vegetation, according to Kadlec and Wallace (2009), which implies that the low N content in the biomass harvested belowground at Wakkerstroom probably was incorrect. As mentioned in section 3.2.3, the C content found in the material harvested belowground was unusually low, probably due to attached mineral material from the sediment, contaminating the samples. The N content was probably incorrect for these belowground samples, for the same reason.

As described in section 2.1.1, net mineralization of dead vegetative material generally occurs when the C:N ratio is below 30. The mean C:N ratio for the aboveground *Phragmites* community was 50.7 ± 24.9 , and 60.4 ± 26.4 for the aboveground *Typha* community (Tab. 6), which implies that the major part of the biomass will probably accumulate as peat and thus create accretions containing organic nitrogen.

5.2.1 Nitrogen uptake

The nitrogen uptake of the vegetation in the Wakkerstroom wetland was estimated to be between 6.10-20.5 g N·m⁻² per growing season (Tab. 11), with an average of 13.0 g N·m⁻² per growing season. Kadlec and Wallace (2009) report the nitrogen uptake to be around 120 g N·m⁻² per growing season as a benchmark for wetlands.

A reason behind the difference between the results obtained in this study and the benchmark value could be due to underestimation of N content in the wetland vegetation. The belowground compartments tend to contain a higher fraction of nutrients and carbon compared to the rest of the plant in the end of the growing season. During senescence, about 50 % of the nitrogen in the ageing tissue is transported to the roots for storage until next growing period (Chapin et al. 2011). The N content in the belowground material harvested in this study was therefore likely to contain a higher N fraction than the aboveground biomass. When only using the mean N content found in the aboveground material for calculating nitrogen uptake, the N content was probably a bit low to represent all the compartments of the vegetation. Since the nitrogen uptake of the Wakkerstroom vlei was estimated by multiplying N content with NPP, another potential reason for the apparently low nitrogen uptake of the wetland is that the LUE model underestimated the production of the wetland, as discussed in section 5.1.3.

However, the production of the Wakkerstroom vlei found in this study is shown to be in a reasonable range, along with the N content found in the biomass harvested aboveground, thus is the estimated nitrogen uptake probably not too far off from the actual uptake, despite the difference compared to the benchmark, which is a general value for all the different types of wetlands.

6. CONCLUSIONS

The NPP_{tot} based on harvested biomass ($NPP_{harvest}$) towards the end of the growing season 2018/2019 was estimated to be $2.01 \text{ kg}\cdot\text{m}^{-2}\cdot\text{season}^{-1}$, which implies that the Wakkerstroom vlei belongs to the more productive wetlands. This amounts to 8353 megagrams (Mg) $\cdot\text{season}^{-1}$ for the whole Wakkerstroom vlei, with an extent of 416 ha. The NPP_{tot} calculated from LUE modelling (NPP_{LUE}) varied between $0.49\text{-}1.64 \text{ kg}\cdot\text{m}^{-2}$ and 2033-6818 Mg for the whole wetland for the growing seasons between 2000-2018, with an 18-year standard error of 10 %. $NPP_{harvest}$ was between 1.2-4 times higher compared to NPP_{LUE} , probably due to overestimation of $NPP_{harvest}$ because of biomass sampling of more than one-year production, or underestimation of NPP_{LUE} due to a low maximum conversion efficiency factor, ϵ_{max} .

The community mean nitrogen (N) content found in the biomass harvested aboveground was 1.29 % for the *Phragmites* community and 1.00 % for the *Typha* community. The community mean N content in the belowground material was 0.57 % for the *Phragmites* community and 0.70 % for the *Typha* community, which probably was too low due to contamination by mineral material. The mean C:N ratio for the aboveground *Phragmites* community was 50.7, and 60.4 for the aboveground *Typha* community, which implies that the majority of the wetland vegetation is likely to accumulate as peat, and thus bury the organic nitrogen rather than make it undergo net mineralization.

The nitrogen uptake of the vegetation was estimated to vary between $6.10\text{-}20.5 \text{ g N}\cdot\text{m}^{-2}$ ($25.4\text{-}85.0 \text{ Mg N}$ for the whole Wakkerstroom vlei) per growing season between the years 2000-2018, which is thought to be quite close to the actual nitrogen uptake of the wetland, since the estimates of the NPP and N content on which it is based are quite defensible relative to published values.

REFERENCES

- Almorox, J., Benito, M. and Hontoria, C. (2004). Estimation of monthly Angström-Prescott equation coefficients from measured daily data in Toledo, Spain. *Renewable Energy*. 30(2005), pp. 931-936. Doi: 10.1016/j.renene.2004.08.002
- Atmospheric Science Data Center (2019). *MISR Frequently Asked Questions*. <https://eosweb.larc.nasa.gov/faq-page/misr-faq#t81n191> (Accessed: 2019-03-27)
- Chapin, F.S.III, Matson, P.A. and Vitousek, P.M. (2011). *Principles of Terrestrial Ecosystem Ecology*. 2nd ed. New York: Springer
- Cofer, W.R.III, Levine, J.S., Winstead, E.L., Lebel, P.J., Koller, A.M.Jr. and Hinkle, R. (1990). Trace Gas Emissions From Burning Florida Wetlands. *Journal of Geophysical Research*. 95(D2), pp. 1865-1870
- Coops, N.C., Hilker, T., Hall, F.G., Nichol, C.J. and Drolet, G.G. (2010). Estimation of Light Use Efficiency of Terrestrial Ecosystems from Space: A status report. *BioScience*. 60(10), pp. 788-797
- Copernicus Global Land Service. *Fraction of Absorbed Photosynthetically Active Radiation*. <https://land.copernicus.eu/global/products/fapar> (Accessed: 2019-02-20)
- Copernicus Sentinel Data (2019). Image derived: 2019-03-20. Downloaded from: <https://earthexplorer.usgs.gov/> (Accessed: 2019-03-28)
- Diner, D.J., Martonchik, J.V., Borel, C., Gerstl, S.A.W., Gordon, H.R., Knyazikhin, Y., Myneni, R., Pinty, B. and Verstraete, M.M. (2008). *Level 2 Surface Retrieval Algorithm Theoretical Basis*. Jet Propulsion Laboratory (JPL D-11401, Revision E) https://eosps0.gsfc.nasa.gov/sites/default/files/atbd/ATB_L2Surface43.pdf (Accessed: 2019-02-22)
- Duffie, J.A. and Beckman, W.A. (2014). *Solar Engineering of Thermal Processes*. 4th ed. New Jersey: John Wiley and Sons, Inc.
- Ellery, W.N. and Joubert, R. (2013). Controls on the formation of Wakkerstroom Vlei, Mpumalanga province, South Africa. *African Journal of Aquatic Science*. 38(2), pp. 135-151. Doi: 10.2989/16085914.2012.762897
- Eriksson, J., Dahlin, S, Nilsson, I. and Simonsson, M. (2011) *Marklära*. 1st ed. Lund: Studentlitteratur
- Germishuizen, G. and Meyer, N.L. (eds) (2003). *Plants of southern Africa: an annotated checklist*. Strelitzia 14. Pretoria: National Botanical Institute
- Gitelson, A.A., Peng, Y., Arkebauer, T.J. and Suyker, A.E. (2015). Productivity, absorbed photosynthetically active radiation, and Light Use Efficiency in crops: Implications for remote sensing of crop primary production. *Journal of Plant Physiology*. 177, pp. 100-109

- Google Earth (2019a). Version 1.3.33.34. Original image: 2015-12-14. Eye alt: 160.7 km. Landsat/Copernicus. (Accessed: 2019-05-10)
- Google Earth (2019b). Version 1.3.33.34. Original image: 2015-12-14. Eye alt: 888.7 km. Landsat/Copernicus. (Accessed: 2019-04-25)
- Google Earth (2019c). Version 1.3.33.34. Original image: 2015-12-14. Eye alt: 11002 km. Landsat/Copernicus and IBCAO. (Accessed: 2019-04-25)
- ITACA (2019-04-19). *Part 3: Calculating Solar Angles*. <https://www.itacanet.org/the-sun-as-a-source-of-energy/part-3-calculating-solar-angles/> (Accessed: 2019-04-19)
- Jaffe, D.A. (1992). The Nitrogen Cycle. In: Butcher, S.S., Charlson, R.J., Orians, G.H. and Wolfe, G.V. (eds), *Global Biogeochemical Cycles*. San Diego: Academic Press Limited
- Jet Propulsion Laboratory. *Mission*. <https://www-misr.jpl.nasa.gov/Mission/> (Accessed: 2019-03-27)
- Kadlec, R.H. and Wallace, S.D. (2009). *Treatment wetlands*. 2nd ed. Taylor and Francis Group
- Kotze, D.C., Breen, C.M. and Klug, J.R. (1994). A management plan for Wakkerstroom Vlei. In: Oellermann, R.G., Darroch, M.A.G., Klug, J.R. and Kotze, D.C. (eds), *Wetland preservation valuation, and management practices applied to wetlands: South African case studies*. WRC Report No. 501/5/94. Pretoria: Water Research Commission
- LAADS DAAC (2019). *Photosynthetically Active Radiation (PAR)*. <https://ladsweb.modaps.eosdis.nasa.gov/missions-and-measurements/products/photosynthetically-active-radiation/> (Accessed: 2019-03-31)
- Liang, S., Li, X. and Wang, J. (2012). *Advanced remote sensing; Terrestrial Information Extraction and Applications*. Oxford: Academic Press
- Liu, Z., Verstraete, M.M. and de Jager, G. (2017). Handling outliers in model inversion studies: a remote sensing case study using MISR-HR data in South Africa. *South African Geographical Journal*. 100(1), pp. 122-139. Doi: 10.1080/03736245.2017.1339629
- Meuleman, A.F.M., Beekman, J.P. and Verhoeven, J.T.A. (2002). Nutrient retention and nutrient-use efficiency in *Phragmites australis* stands after wastewater application. *Wetlands*. 22(4), pp. 712-721. Doi: 10.1672/0277-5212
- MISR-HR (2015a). *Inputs to the MISR-HR processing system*. <http://www.misrhr.org/inputs> (Accessed: 2019-03-20)

- MISR-HR (2015b). *MISR-HR Products*. <http://www.misrhr.org/outputs> (Accessed: 2019-03-20)
- MISR-HR (2018). *Overview of the MISR-HR processing system*. <http://www.misrhr.org/overview> (Accessed: 2019-03-20)
- MISR-HR (2019). *MISR-HR JRC-TIP Product*. <http://www.misrhr.org/tip> (Accessed: 2019-03-20)
- Mitsch, W.J. and Gosselink, J.G. (2015). *Wetlands*. 5th ed. New Jersey: Wiley
- Moyo, M.S. (2015). *Long Term Climate Analysis for Volksrust*. Honours project, University of the Witwatersrand, Johannesburg
- Mulaudzi, S.T., Sankaran, V. and Lysko, M.D. (2013). Solar radiation analysis and regression coefficients for the Vhembe Region, Limpopo Province, South Africa. *Journal of Energy in Southern Africa*. 24(3), pp. 2-7. Doi: 10.17159/2413-3051/2014/v24i3a3136
- Nuarsa, I.W., As-syakur, A.R., Gunadi, I.G.A. and Sukewijaya, I.M. (2018). Changes in Gross Primary Production (GPP) over the past Two decades Due to Land Use Converison in a Toursim City. *International Journal of Geo-Information*. 7(2). Doi: 10.3390/ijgi7020057
- Numerical Terradynamic Simulation Group (2019-02-21). *MODIS GPP/NPP Project (MOD17)*. <http://www.ntsug.umd.edu/project/modis/mod17.php> (Accessed: 2019-02-21)
- Oellerman, R.G., Darroch, M.A.G., Klug, J.R. and Kotze, D.C. (1994). Wetland preservation valuation, and management practices applied to wetlands: South African case studies. In: Oellermann, R.G., Darroch, M.A.G., Klug, J.R. and Kotze, D.C. (eds), *Wetland preservation valuation, and management practices applied to wetlands: South African case studies*. WRC Report No. 501/5/94. Pretoria: Water Research Commission
- Packer, J.G., Meyerson, L.A., Skálová, H., Pyšek, P. and Kueffer, C. (2017). Biological Flora of the British Isles: *Phragmites australis*. *Journal of Ecology*. 105(4), pp. 1123–1164
- Pezzullo, J.C. (2013). *Biostatistics For Dummies*. New Jersey: John Wiley and Sons, Inc.
- Ramsey, J.D. (2011). *Statistics For Dummies*. 2nd ed. Indiana: Wiley Publishing, Inc.
- Running, S.W. and Zhao, M. (2015). *User's Guide Daily GPP and Annual NPP (MOD17A2/A3) Products NASA Earth Observing System MODIS Land Algorithm*. https://lpdaac.usgs.gov/sites/default/files/public/product_documentation/mod17_user_guide.pdf (Accessed 2018-09-15)

- Sandusky-Aber, J., Pavri, F. and Ward-Aber, S. (2012). *Wetland Environments: A Global Perspective*. West Sussex: Wiley-Blackwell
- Sentinel (2019-04-18). *Overview*. <https://sentinel.esa.int/web/sentinel/missions/sentinel-2/overview> (Accessed 2019-04-18)
- South African National Biodiversity Institute (2007). *Typha capensis*. <http://pza.sanbi.org/typha-capensis> (Accessed 2019-02-12)
- Swift, M.J., Heal, O.W. and Anderson, J.M. (1979). Decomposition in Terrestrial Ecosystems. In: Anderson, D.J, Greig-Smith, P. and Pitelka, F.A. (eds), *Studies in Ecology. Vol. 5*. Blackwell Scientific Publications
- Thermo Fisher Scientific (2019-05-15). *Thermo Scientific FLASH HT Plus Elemental Analyzer for IRMS; Fully Automated Multi-Element Isotope Analysis for C, N, S O, H*. http://www.ebd.csic.es/lie/PDF/AE_HT_plusPDF_54379.pdf (Accessed 2019-05-15)
- Tjoelker, M.G., Oleksyn, J. and Reich, P.B. (2001). Modelling respiration of vegetation: evidence for a general temperature-dependent Q_{10} . *Global Change Biology*. 7, pp. 223-230
- UNESCO (2017). *2017 UN World Water Development Report, Wastewater: The Untapped Resource*. <http://www.unesco.org/new/en/natural-sciences/environment/water/wwap/wwdr/2017-wastewater-the-untapped-resource/> (Accessed: 2019-03-18)
- United Nations (2018). *The Sustainable Development Goals Report: 2018*. New York: United Nations. <https://unstats.un.org/sdgs/files/report/2018/TheSustainableDevelopmentGoalsReport2018-EN.pdf> (Accessed: 2019-02-28)
- Van der Walk, A.G. (2006). *Biology of Freshwater Wetlands*. New York: Oxford University Press
- Verstraete, M.M., Hunt, L.A., Scholes, R.J., Clerici, M., Pinty, B. and Nelson, D.L. (2012). Generating 275 m Resolution Land Surface Products From the Multi-Angle Imaging SpectroRadiometer Data. *IEEE Transactions on Geoscience and remote sensing*. 50(10), pp. 3980-3990. Doi: 10.1109/TGRS.2012.2189575
- Vrieling, A., de Leeuw, J. and Said, M.Y. (2013). Length of Growing Period over Africa: Variability and Trends from 30 Years of NDVI Time Series. *Remote Sensing*. 5, pp. 982-1000. Doi: 10.3390/rs5020982
- Vymazal, J. and Kröpfelová, L. (2010). Nutrient Accumulation by *Phragmites australis* and *Phalaris arundinacea* Growing in Two Constructed Wetlands for Wastewater Treatment. In: Vymazal, J. (ed), *Water and Nutrient Management in Natural and Constructed Wetlands*. Springer, pp. 133-149. Doi: 10.1007/978-90-481-9585-5_11

- Wardrop, D.H., Fennessy, M.S., Moon, J. and Britson, A. (2016). Effects of Human Activity on the Processing of Nitrogen in Riparian Wetlands: Implications for Watershed Water Quality. In: Vymazal, J. (ed), *Natural and Constructed Wetlands: Nutrients, heavy metals and energy cycling, and flow*. Springer, pp. 1-22
- World Weather Online (2019-04-26). *Volksrust Monthly Climate Averages*. <https://www.worldweatheronline.com/volksrust-weather-averages/mpumalanga/za.aspx> (Accessed: 2019-04-26)
- Yan, H., Wang, S., Billesbach, D., Oechel, W., Bohrer, G., Meyers, T., Martin, T.A., Matamala, R., Phillips, R.P., Rahmna, F., Yu, Q. and Shugart, H.H. (2015). Improved global simulations of gross primary product based on a new definition of water stress factor and a separate treatment of C3 and C4 plants. *Ecological Modelling*. 297, pp. 42-59
- Yuan, W., Cai, W., Xia, J., Chen, J., Liu, S., Dong, W., Merbold, L., Law, B., Arain, A., Beringer, J., Bernhofer, C., Black, A., Blanken, P.D., Cescetti, A., Chen, Y., Francois, L., Gianelle, D., Janssens, I.A., Jung, M., Kato, T., Kiely, G., Liu, D., Marcolla, B., Montagnani, L., Raschi, A., Roupsard, O., Varlagin, A. and Wohlfahrt, G. (2014). Global comparison of Light Use Efficiency models for simulating terrestrial vegetation gross primary production based on the LaThuile database. *Agricultural and Forest Meteorology*. 192-193, pp. 198-120

APPENDIX

A. BIOMASS SAMPLING

Table A1. The latitude and longitude of the sampling locations.

Location	Latitude (S°)	Longitude (E°)
1	-27.346954	30.1399294
2	-27.3444613	30.1415529
3	-27.3400774	30.1427888
4	-27.3455453	30.1286759
5	-27.3460023	30.1287961
6	-27.3528623	30.1229305
7	-27.3615201	30.1201352
8	-27.3629337	30.1225323
9	-27.3639634	30.1253000

Table A2. Sampling date, water depth of the location and wet mass of the harvested biomass samples. Note that the wet mass is for an area of 0.25 m².

Plant community	Sampling date	Sample nr	Water depth [m]	Wet mass [g]
<i>Phragmites</i>	2019-03-10	1	0.2	1615.6
	2019-03-10	2	0.1	1115.4
	2019-03-13	3	0.4	627.3
	2019-03-13	4	0.2	558.2
	2019-03-13	5	0.25	729.5
	2019-03-13	6	0.2	602.7
	2019-03-13	7	0.45	709.2
	2019-03-13	8	0.3	674.5
	2019-03-14	9	0.1	1159.7
	2019-03-14	10	0.2	825.4
	2019-03-14	11	0.1	944.2
	2019-03-14	12	0.1	1464.4
	2019-03-14	13	0.05	1122.2
	2019-03-14	14	0.15	1081.2
	2019-03-15	15	0.05	576.2
	2019-03-15	16	0.1	1102.4
	2019-03-15	17	0.15	488.2
	2019-03-15	18	0.1	432.1
	2019-03-15	19	0.15	692.6
	2019-03-15	20	0.15	566.4
<i>Typha</i>	2019-03-10	1	0.3	839.3
	2019-03-10	2	0.1	2211.0
	2019-03-12	3	0.1	1556.2

2019-03-12	4	0.2	999.5
2019-03-19	5	0.35	1215.5

Table A3. Wet and dry mass of the samples dried in the drying oven.

Plant community	Sample	Wet mass [g]	Dry mass [g]
<i>Phragmites</i>	P1	1615.6	412.4
	P2	1115.4	325.0
	P3	627.3	362.2
	P4	558.2	301.5
	P5	729.5	426.5
	Total	4646.0	1827.6
<i>Typha</i>	T1	839.3	188.4
	T2	2211.0	459.2
	T3	1556.2	541.0
	Total	4606.5	1188.6

Table A4. Sampling date, wet and dry mass of the aboveground (AG_{RF}) and belowground (BG) biomass samples. The sample names containing AG refers to AG_{RF}.

Plant community	Sampling date	Sample	Wet mass [g]	Dry mass [g]
<i>Phragmites</i>	2019-03-22	PAG1	85.9	-
	2019-03-22	PAG2	156.0	-
	2019-03-23	PAG3	81.6	-
	2019-03-23	PAG4	110.6	-
	2019-03-23	PAG5	68.5	-
	Total	-	502.6	197.5*
	2019-03-22	PBG1	36.3	8.0
	2019-03-22	PBG2	152.2	32.0
	2019-03-23	PBG3	40.0	8.3
	2019-03-23	PBG4	296.6	80
	2019-03-23	PBG5	37.2	7.0
	Total	-	562.3	135.3
<i>Typha</i>	2019-03-22	TAG1	97.2	-
	2019-03-22	TAG2	80.0	-
	2019-03-22	TAG3	114.9	-
	2019-03-22	TAG4	114.6	-
	2019-03-22	TAG5	110.8	-
	Total	-	517.5	133.5*
	2019-03-22	TBG1	125.1	17.4

2019-03-22	TBG2	353.8	61.6
2019-03-22	TBG3	292.7	37.4
2019-03-22	TBG4	296.6	24.1
2019-03-22	TBG5	550.8	108.3
Total	-	1619.0	248.8

* The dry mass calculated by multiplying the wet mass with the DM content, see Tab. 7 in section 4.2.1.

Table A5. Calculation steps for deriving root fraction (RF). The BG biomass was assumed to have the same C content as the AG biomass. Based on this assumption, a mineral correction factor (MCF) was derived and a corrected dry mass for the BG biomass was calculated. RF was obtained from Eq. 2 with the AG_{RF} dry mass and corrected BG dry mass.

Plant community	Dry mass, AG_{RF} [g]	Dry mass, BG [g]	C content, BG [%]	C content, AG [%]	MCF [-]	Corrected dry mass, BG [g]	RF [-]
<i>Phragmites</i>	197.5	135.3	18.6	43.8	0.425	57.5	0.23
<i>Typha</i>	133.5	248.8	36.9	44.2	0.835	207.7	0.61

B. FAPAR

Table B1. The latitude and longitude of the points used for finding a suitable MISR block and pixels for the Wakkerstroom wetland.

Point	Latitude [°S]	Longitude [°E]
1	-27.34439555	30.13553714
2	-27.34681798	30.13414477
3	-27.34916228	30.13279724
4	-27.35170186	30.1313374
5	-27.35412394	30.12994504
6	-27.35646821	30.12859735
7	-27.35881247	30.1272496
8	-27.36115673	30.1259018
9	-27.36352877	30.12453797
10	-27.36587272	30.12319023
11	-27.36821694	30.12184227

Table B2. The latitude and longitude coordinates in degrees of the northwest (NW), northeast (NE), southwest (SW) and southeast (SE) corners of the pixels used for extracting FAPAR from Path 168.

Pixel	NW [°S;°E]	NE [°S;°E]	SW [°S;°E]	SE [°S;°E]
1	-27.34263584; 30.13557355	-27.34290850; 30.13833548	-27.34510221; 30.13526804	-27.34537488; 30.13803003
2	-27.34482949; 30.13250606	-27.34510221; 30.13526804	-27.34729586; 30.13220048	-27.34756859; 30.13496251
3	-27.34729586; 30.13220048	-27.34756859; 30.13496251	-27.34976222; 30.13189488	-27.35003496; 30.13465697
4	-27.34948943; 30.1291328	-27.34976222; 30.13189488	-27.35195578; 30.12882712	-27.35222858; 30.13158926
5	-27.35195578; 30.12882712	-27.35222858; 30.13158926	-27.35442214; 30.12852143	-27.35469495; 30.13128363
6	-27.35442214; 30.12852143	-27.35469495; 30.13128363	-27.35688849; 30.12821572	-27.35716131; 30.13097799
7	-27.35661562; 30.12545348	-27.35688849; 30.12821572	-27.35908196; 30.12514769	-27.35935484; 30.12791

8	-27.35908196; 30.12514769	-27.35935484; 30.12791	-27.3615483; 30.1248419	-27.36182119; 30.12760426
9	-27.36127536; 30.12207954	-27.3615483; 30.1248419	-27.3637417; 30.12177367	-27.36401464; 30.12453608
10	-27.3637417; 30.12177367	-27.36401464; 30.12453608	-27.36620803; 30.12146778	-27.36648098; 30.12423025
11	-27.36620803; 30.12146778	-27.36648098; 30.12423025	-27.36867436; 30.12116187	-27.36894732; 30.12392441

Table B3. *The latitude and longitude coordinates in degrees of the centre of the pixels in path 168, and the distance between the centre of each pixel and the corresponding point of interest covering the Wakkerstroom wetland.*

Pixel	Centre of pixel [°S;°E]	Distance [m]
1	-27.34400537; 30.13680177	132.2
2	-27.34619904; 30.13373427	79.9
3	-27.34866541; 30.13342871	83.3
4	-27.35085901; 30.13036101	134.5
5	-27.35332537; 30.13005536	89.5
6	-27.35579173; 30.12974969	136.4
7	-27.35798523; 30.12668172	107.7
8	-27.36045158; 30.12637596	91.3
9	-27.36264501; 30.12330780	156.3
10	-27.36511134; 30.12300195	86.7
11	-27.36757768; 30.12269608	110.3

C. PAR

Table C1. The monthly hours of sunshine obtained from World Weather Online (2019-04-26) for the time period 2009-2017.

Year	Month	Nr of hours/month	Days of the month	Hours of sunshine/day
2009	Jan	300	31	9.7
2009	Feb	250.5	28	8.9
2009	Mar	267	31	8.6
2009	Apr	211	30	7.0
2009	Maj	230	31	7.4
2009	Jun	210.5	30	7.0
2009	Jul	231	31	7.5
2009	Aug	223.5	31	7.2
2009	Sep	247	30	8.2
2009	Okt	310.5	31	10.0
2009	Nov	316.5	30	10.6
2009	Dec	339	31	10.9
2010	Jan	264.5	31	8.5
2010	Feb	296	28	10.6
2010	Mar	286	31	9.2
2010	Apr	203	30	6.8
2010	Maj	228.5	31	7.4
2010	Jun	223.5	30	7.5
2010	Jul	227	31	7.3
2010	Aug	232.5	31	7.5
2010	Sep	265	30	8.8
2010	Okt	356	31	11.5
2010	Nov	340.5	30	11.4
2010	Dec	351	31	11.3
2011	Jan	314	31	10.1
2011	Feb	328	28	11.7
2011	Mar	318.5	31	10.3
2011	Apr	214.5	30	7.2
2011	Maj	226.5	31	7.3
2011	Jun	219	30	7.3
2011	Jul	228	31	7.4
2011	Aug	226.5	31	7.3
2011	Sep	262	30	8.7
2011	Okt	372.5	31	12.0
2011	Nov	355.5	30	11.9
2011	Dec	356.5	31	11.5
2012	Jan	347.5	31	11.2
2012	Feb	330.5	29	11.4
2012	Mar	321.5	31	10.4

2012	Apr	222.5	30	7.4
2012	Maj	323.5	31	10.4
2012	Jun	222.5	30	7.4
2012	Jul	232.5	31	7.5
2012	Aug	229.5	31	7.4
2012	Sep	244	30	8.1
2012	Okt	365	31	11.8
2012	Nov	347.5	30	11.6
2012	Dec	355	31	11.5
2013	Jan	327.5	31	10.6
2013	Feb	322	28	11.5
2013	Mar	308	31	9.9
2013	Apr	207.5	30	6.9
2013	Maj	229.5	31	7.4
2013	Jun	223.5	30	7.5
2013	Jul	232.5	31	7.5
2013	Aug	231	31	7.5
2013	Sep	259	30	8.6
2013	Okt	372.5	31	12.0
2013	Nov	351.5	30	11.7
2013	Dec	347	31	11.2
2014	Jan	358	31	11.5
2014	Feb	318	28	11.4
2014	Mar	270	31	8.7
2014	Apr	225	30	7.5
2014	Maj	222.5	31	7.2
2014	Jun	225	30	7.5
2014	Jul	232.5	31	7.5
2014	Aug	229.5	31	7.4
2014	Sep	259	30	8.6
2014	Okt	369.5	31	11.9
2014	Nov	358	30	11.9
2014	Dec	356.5	31	11.5
2015	Jan	371	31	12.0
2015	Feb	341	28	12.2
2015	Mar	305	31	9.8
2015	Apr	210	30	7.0
2015	Maj	231	31	7.5
2015	Jun	225	30	7.5
2015	Jul	220.5	31	7.1
2015	Aug	232.5	31	7.5
2015	Sep	232.5	30	7.8
2015	Okt	368	31	11.9
2015	Nov	356.5	30	11.9
2015	Dec	364	31	11.7
2016	Jan	356.5	31	11.5

2016	Feb	350.5	29	12.1
2016	Mar	302.5	31	9.8
2016	Apr	192.5	30	6.4
2016	Maj	222	31	7.2
2016	Jun	220.5	30	7.4
2016	Jul	217.5	31	7.0
2016	Aug	232.5	31	7.5
2016	Sep	249	30	8.3
2016	Okt	377	31	12.2
2016	Nov	362	30	12.1
2016	Dec	367.5	31	11.9
2017	Jan	339.5	31	11.0
2017	Feb	291	28	10.4
2017	Mar	323.5	31	10.4
2017	Apr	223.5	30	7.5
2017	Maj	211.5	31	6.8
2017	Jun	225	30	7.5
2017	Jul	232.5	31	7.5
2017	Aug	231	31	7.5
2017	Sep	261.5	30	8.7
2017	Okt	370	31	11.9
2017	Nov	352	30	11.7
2017	Dec	355.5	31	11.5

D. CONVERSION EFFICIENCY FACTOR ε

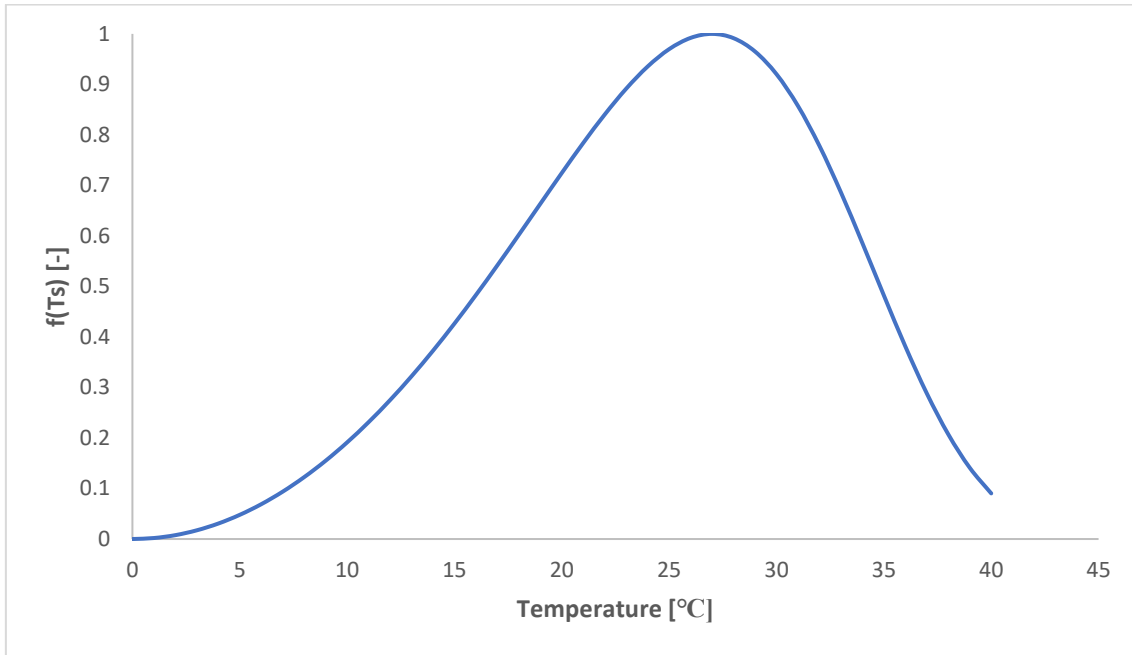


Figure D1. The calibration graph used for determining the values of the slope parameters, c and d , used in the function $f(T_s)$.

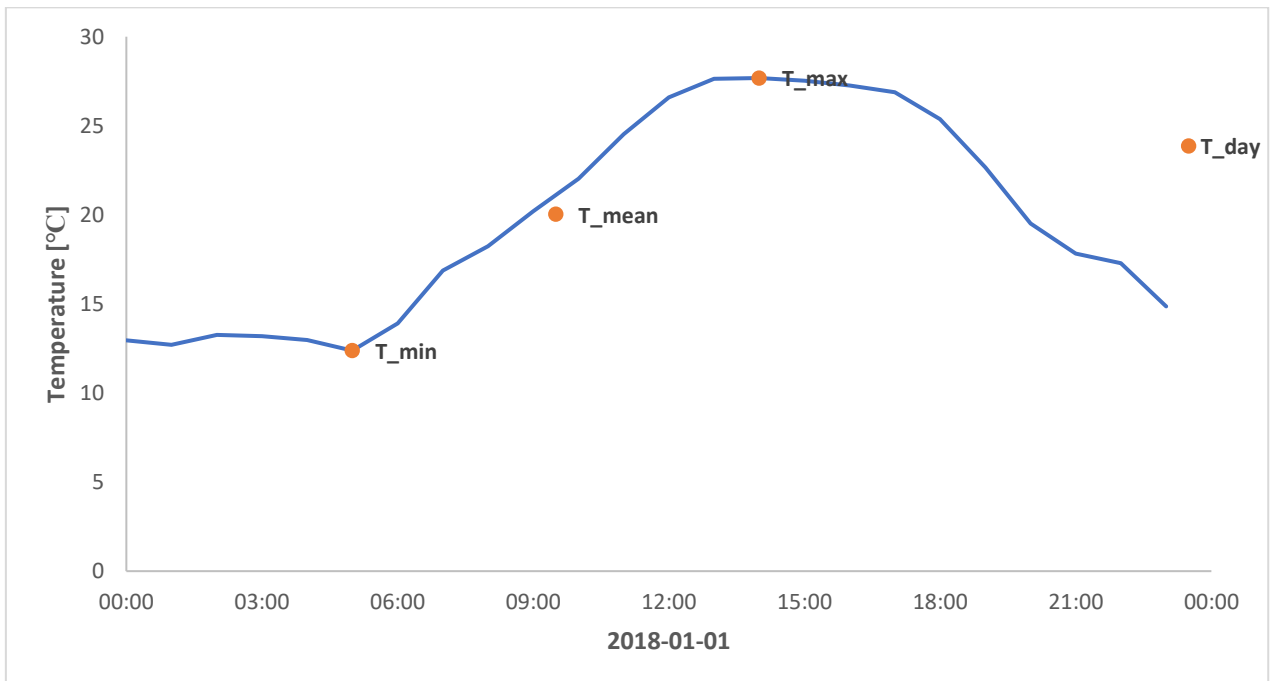


Figure D2. The hourly temperature curve for 2018-01-01, displaying the minimum temperature (T_{min}), maximum temperature (T_{max}), mean temperature (T_{mean}) and mean temperature for the daytime (T_{day}) in orange.

E. NPP

Table E1. NPP_{tot} calculated from LUE modelling per area unit with standard deviation (*std.dev*) and mean, for pixel 1-11, during the growing seasons between the years 2000-2018.

Pixel	1	2	3	4	5	6	7	8	9	10	11		
Growing season	NPP_{tot}	Mean	Std.dev										
	[kg/m ²]	[kg/m ²]	[kg/m ²]										
2000/2001	0.625	0.643	0.628	0.613	0.613	0.612	0.610	0.604	0.603	0.605	0.605	0.615	0.013
2001/2002	0.638	0.661	0.657	0.645	0.641	0.643	0.646	0.641	0.634	0.620	0.624	0.641	0.012
2002/2003	0.669	0.675	0.669	0.658	0.652	0.632	0.658	0.659	0.651	0.626	0.622	0.652	0.018
2003/2004	0.682	0.690	0.681	0.676	0.674	0.675	0.679	0.676	0.671	0.670	0.668	0.677	0.006
2004/2005	0.678	0.681	0.680	0.678	0.680	0.688	0.682	0.678	0.673	0.678	0.678	0.679	0.004
2005/2006	0.636	0.665	0.665	0.664	0.673	0.642	0.657	0.346	0.653	0.653	0.648	0.627	0.094
2006/2007	0.766	0.726	0.722	0.712	0.743	0.746	0.725	0.385	0.729	0.727	0.730	0.701	0.106
2007/2008	0.510	0.505	0.500	0.490	0.479	0.486	0.481	0.469	0.479	0.503	0.482	0.489	0.013
2008/2009	1.097	1.111	1.102	1.091	1.088	1.095	1.092	1.082	1.074	1.080	1.083	1.090	0.011
2009/2010	1.357	1.377	1.354	1.344	1.341	1.361	1.322	1.306	1.319	1.317	1.300	1.336	0.025
2010/2011	1.512	1.563	1.459	1.486	1.630	1.641	1.519	1.523	1.511	1.494	1.535	1.534	0.057
2011/2012	1.540	1.657	1.589	1.640	1.627	1.546	1.670	1.658	1.628	1.655	1.634	1.622	0.045
2012/2013	1.537	1.542	1.543	1.524	1.523	1.514	1.501	1.491	1.526	1.554	1.538	1.526	0.019
2013/2014	1.494	1.570	1.532	1.550	1.473	1.498	1.418	1.414	1.446	1.458	1.448	1.482	0.052
2014/2015	1.083	1.118	1.183	1.144	0.934	0.925	0.792	0.869	1.164	1.252	1.103	1.052	0.147
2015/2016	1.270	1.286	1.216	1.195	1.202	1.205	1.090	1.047	1.058	1.022	1.283	1.170	0.099
2016/2017	1.691	1.681	1.667	1.530	1.668	1.678	1.676	1.667	1.649	1.653	1.491	1.641	0.066
2017/2018	1.242	1.229	1.227	1.237	1.245	1.250	1.244	1.233	1.202	1.221	1.222	1.232	0.014

F. CARBON AND NITROGEN CONTENT

Project ID: APES041		Name: Emma Dufbück				Date: 2019-05-10					
Identifier	Amount	Area 28	d 15N/14N	Area 44	d 13C/12C	15N corr	±N	13Ccorr	±C	C/N	
P 1/5	0.53	6.96	10.68	414.22	-25.71	10.98	2.10	-26.01	44.40	24.72	
P 1/5	0.67	8.91	10.86	537.74	-26.22	11.15	2.11	-27.23	45.30	25.07	
P 1/5	0.57	8.05	11.25	458.26	-25.72	11.51	2.24	-26.25	45.40	23.65	
P 1/5	0.61	7.45	10.78	463.64	-27.60	11.08	1.94	-28.36	42.91	25.87	
P 1/5	0.52	6.89	10.09	397.64	-26.02	10.45	2.11	-26.27	43.28	23.98	
P 7/1	0.46	2.55	4.44	352.40	-26.28	5.24	0.88	-26.32	43.20	57.39	
P 7/1	0.59	3.06	5.44	461.44	-26.24	6.16	0.82	-26.84	43.94	62.69	
P 7/1	0.70	3.64	5.17	551.58	-27.15	5.92	0.82	-28.33	44.41	63.02	
P 7/1	0.56	2.98	4.97	439.78	-26.85	5.73	0.84	-27.40	43.96	61.25	
P 7/1	0.52	2.45	6.07	399.80	-26.51	6.74	0.74	-26.82	43.35	67.91	
P 9/5	0.68	5.63	6.22	548.11	-26.74	6.88	1.31	-27.86	45.36	40.48	
P 9/5	0.58	3.46	5.83	462.22	-26.74	6.53	0.94	-27.40	44.77	55.44	
P 9/5	0.52	2.60	4.88	413.11	-26.80	5.65	0.79	-27.21	44.37	65.94	
P 9/5	0.64	4.27	5.94	488.29	-26.41	6.62	1.05	-27.17	42.80	47.48	
P 9/5	0.52	3.76	5.66	405.48	-26.89	6.36	1.15	-27.27	44.14	44.86	
P 13/1	0.65	8.40	4.99	507.54	-26.95	5.75	2.03	-27.88	43.74	25.09	
P 13/1	0.52	6.17	4.71	404.12	-27.13	5.49	1.87	-27.52	43.73	27.22	
P 13/1	0.66	9.58	4.65	502.85	-27.62	5.43	2.31	-28.59	43.20	21.80	
P 13/1	0.65	7.90	4.80	466.31	-27.27	5.57	1.92	-28.01	40.31	24.51	
P 13/1	0.56	5.19	4.19	434.56	-29.31	5.01	1.46	-30.10	43.59	34.80	
P 19/2	0.55	2.11	0.42	430.14	-27.93	1.54	0.60	-28.56	43.85	84.90	
P 19/2	0.69	2.48	2.09	529.99	-28.71	3.08	0.57	-29.95	43.22	88.86	
P 19/2	0.59	2.26	-0.16	466.16	-30.14	1.01	0.60	-31.19	44.16	85.88	
P 19/2	0.65	2.08	0.32	497.59	-27.92	1.45	0.51	-28.89	43.08	99.34	
P 19/2	0.65	2.50	-0.67	506.28	-26.91	0.54	0.61	-27.82	44.04	84.27	
T 1/1	0.45	3.98	8.68	354.36	-30.25	9.15	1.39	-30.72	44.12	36.98	
T 1/1	0.68	6.63	9.05	535.17	-30.74	9.49	1.54	-32.22	44.29	33.54	
T 1/1	0.57	5.37	9.10	445.96	-29.13	9.53	1.49	-29.96	44.18	34.52	
T 1/1	0.49	4.15	9.36	385.25	-29.43	9.77	1.33	-29.98	43.97	38.60	
T 1/1	0.67	5.08	8.74	516.15	-30.28	9.20	1.21	-31.60	43.61	42.21	
T 2/3	0.43	3.57	8.12	342.36	-27.92	8.63	1.31	-28.07	44.60	39.85	
T 2/3	0.64	5.47	9.40	511.56	-26.34	9.81	1.36	-27.23	45.26	38.85	
T 2/3	0.61	5.38	8.96	488.74	-27.36	9.41	1.39	-28.24	45.01	37.73	
T 2/3	0.52	4.56	8.80	414.53	-26.81	9.25	1.39	-27.23	44.86	37.76	
T 2/3	0.55	4.31	8.87	433.04	-26.97	9.33	1.24	-27.51	44.47	41.72	
T 3/2	0.51	1.49	3.11	402.75	-27.93	4.02	0.46	-28.41	44.18	112.00	
T 3/2	0.68	2.32	3.11	546.00	-27.05	4.02	0.54	-28.19	44.92	97.69	
T 3/2	0.61	1.95	1.35	480.30	-28.23	2.40	0.51	-29.15	44.38	102.23	
T 3/2	0.60	1.96	2.94	466.80	-27.41	3.86	0.52	-28.17	44.15	99.10	
T 3/2	0.44	1.74	1.14	351.16	-27.98	2.20	0.62	-28.19	44.51	83.94	
T 4/1	0.52	2.71	2.69	460.05	-29.19	3.63	0.83	-30.10	50.27	70.61	
T 4/1	0.61	2.98	3.34	480.28	-28.14	4.22	0.77	-29.04	44.16	66.87	
T 4/1	0.52	2.08	2.94	412.03	-29.83	3.86	0.63	-30.56	44.42	82.26	
T 4/1	0.51	1.82	1.06	394.48	-28.68	2.13	0.57	-29.19	43.87	90.30	
T 4/1	0.49	1.70	1.53	378.58	-29.30	2.56	0.55	-29.79	43.48	92.79	
T 5/3	0.55	4.44	8.66	420.62	-29.38	9.13	1.27	-30.10	42.88	39.34	
T 5/3	0.51	4.33	9.22	388.50	-29.23	9.64	1.33	-29.76	42.53	37.29	
T 5/3	0.51	3.46	8.85	378.76	-28.26	9.31	1.08	-28.64	41.96	45.45	
T 5/3	0.51	3.06	9.15	377.21	-28.42	9.58	0.95	-28.81	41.87	51.23	
T 5/3	0.50	2.69	8.63	372.08	-28.03	9.10	0.85	-28.35	41.79	57.42	
TB 1	0.47	2.75	6.18	308.70	-28.96	6.85	0.92	-29.05	36.65	46.71	
TB 1	0.63	3.57	6.20	412.75	-30.28	6.86	0.90	-31.06	37.04	48.06	
TB 1	0.47	2.64	8.07	306.37	-29.27	8.59	0.89	-29.38	36.68	48.14	
TB 1	0.46	2.55	6.87	311.22	-28.73	7.48	0.87	-28.81	37.74	50.78	
TB 1	0.62	3.70	6.92	411.08	-28.20	7.52	0.94	-28.75	37.13	46.21	
TB 2	0.62	3.25	6.58	386.16	-28.90	7.21	0.83	-29.39	35.11	49.42	
TB 2	0.55	2.74	7.26	352.11	-28.57	7.84	0.78	-28.84	35.83	53.33	
TB 2	0.57	2.52	6.77	375.14	-28.32	7.39	0.70	-28.69	37.04	61.85	
TB 2	0.56	2.68	6.45	362.79	-28.66	7.10	0.75	-29.00	36.39	56.26	
TB 2	0.49	2.17	7.16	316.19	-27.97	7.75	0.70	-27.99	36.09	60.54	

Project ID: APES041		Name: Emma Dufbück				Date: 2019-05-10					
Identifiser	Amount	Area 28	d 15N/14N	Area 44	d 13C/12C	15N corr	13Ccorr	13C	C/N		
TB 3	0.43	1.23	6.58	284.49	-27.35	7.22	0.46	-27.14	37.49	95.94	
TB 3	0.52	1.52	7.59	351.97	-28.11	8.14	0.46	-28.34	38.02	96.08	
TB 3	0.54	1.46	4.33	365.19	-28.29	5.14	0.42	-28.61	37.85	104.06	
TB 3	0.59	1.76	6.79	398.51	-27.87	7.41	0.47	-28.32	38.14	94.34	
TB 3	0.65	1.86	7.37	424.14	-27.14	7.94	0.45	-27.65	36.83	94.94	
TB 4	0.42	1.97	4.89	276.17	-28.22	5.66	0.74	-28.06	36.83	58.15	
TB 4	0.55	2.49	5.71	360.31	-28.34	6.41	0.71	-28.63	36.60	60.07	
TB 4	0.45	2.08	5.64	295.18	-29.21	6.35	0.72	-29.25	36.67	59.04	
TB 4	0.48	2.20	6.34	315.26	-27.88	6.99	0.73	-27.88	37.04	59.53	
TB 4	0.63	3.08	6.92	414.35	-27.73	7.53	0.78	-28.24	37.13	55.87	
TB 5	0.53	2.11	6.13	335.44	-27.29	6.80	0.63	-27.35	35.68	66.17	
TB 5	0.58	2.56	7.23	386.99	-27.43	7.82	0.70	-27.77	37.68	62.71	
TB 5	0.47	1.98	7.17	305.20	-27.20	7.76	0.67	-27.08	36.86	64.20	
TB 5	0.47	2.07	6.67	310.42	-27.45	7.30	0.70	-27.38	37.41	62.18	
TB 5	0.51	2.19	6.11	327.47	-27.57	6.78	0.68	-27.61	36.28	62.07	
PB 1	0.54	2.55	6.31	241.55	-26.87	6.97	0.74	-26.37	24.99	39.32	
PB 1	0.55	2.49	5.39	203.45	-26.80	6.12	0.71	-26.09	20.67	33.99	
PB 1	0.63	3.19	6.71	248.98	-27.18	7.33	0.80	-26.76	22.27	32.39	
PB 1	0.56	2.88	6.64	275.60	-26.85	7.27	0.81	-26.54	27.50	39.81	
PB 1	0.58	2.75	5.71	226.99	-26.64	6.41	0.75	-26.05	21.95	34.34	
PB 2	0.47	1.75	5.45	191.49	-26.08	6.18	0.58	-25.24	22.78	45.49	
PB 2	0.61	2.03	5.36	216.92	-26.35	6.09	0.52	-25.67	20.01	44.50	
PB 2	0.56	1.78	4.87	212.87	-26.69	5.64	0.51	-26.03	21.55	49.71	
PB 2	0.62	2.17	5.92	288.21	-26.40	6.60	0.55	-26.11	25.99	55.18	
PB 2	0.47	1.56	3.57	170.40	-26.29	4.44	0.53	-25.36	20.40	45.27	
PB 3	0.51	1.73	5.82	153.47	-26.02	6.51	0.54	-24.97	16.97	36.94	
PB 3	0.48	1.71	4.86	182.30	-25.83	5.63	0.57	-24.91	21.60	44.32	
PB 3	0.58	2.06	4.96	184.60	-26.12	5.72	0.56	-25.24	17.94	37.19	
PB 3	0.53	1.92	5.65	218.25	-26.44	6.35	0.57	-25.78	23.09	47.13	
PB 3	0.57	2.10	4.92	203.99	-25.83	5.69	0.58	-25.03	20.14	40.28	
PB 4	0.61	1.97	6.55	167.22	-25.55	7.19	0.51	-24.53	15.33	35.34	
PB 4	0.43	1.44	3.88	127.88	-25.60	4.73	0.53	-24.37	16.70	36.82	
PB 4	0.61	1.79	4.72	145.59	-25.22	5.50	0.47	-24.05	13.48	33.74	
PB 4	0.64	1.97	6.56	193.14	-25.55	7.20	0.49	-24.66	17.09	40.67	
PB 4	0.54	1.88	5.12	185.26	-26.14	5.87	0.55	-25.27	19.16	40.94	
PB 5	0.61	1.95	4.26	127.39	-25.93	5.08	0.50	-24.73	11.68	27.20	
PB 5	0.55	1.71	3.09	107.38	-26.47	4.00	0.49	-25.22	10.95	26.07	
PB 5	0.56	1.78	3.25	103.03	-25.25	4.14	0.50	-23.86	10.34	24.06	
PB 5	0.47	1.33	1.94	83.44	-24.91	2.94	0.45	-23.37	9.95	26.06	
PB 5	0.65	2.05	4.05	141.26	-25.78	4.89	0.50	-24.65	12.25	28.61	
Identifiser	Amount	Area 28	d 15N/14N	Area 44	d 13C/12C	15N corr	13Ccorr				
Merck	0.26	22.43	6.02	190.48	-21.73	6.68	-20.43				
Merck	0.26	22.87	6.17	192.67	-21.89	6.83	-20.62				
Merck	0.41	36.80	6.21	310.99	-21.58	6.85	-20.89				
Merck	0.61	56.24	6.24	473.68	-20.41	6.87	-20.47				
Merck	0.60	55.39	6.17	467.35	-20.29	6.81	-20.29				
Merck	0.81	77.12	6.28	653.30	-19.61	6.90	-20.54				
Merck	0.81	77.84	6.27	659.08	-19.97	6.89	-20.97				
Merck	0.81	82.60	5.93	671.04	-19.35	6.57	-20.34				
					Ref. value	6.80	-20.57				
					Precision	0.11	0.25				
UREA	0.30	88.99	-2.05	111.61	-40.01	-0.78	-40.22				
UREA	0.31	91.61	-1.94	115.27	-39.10	-0.68	-39.23				
					Ref. value	-0.73	-39.73				
					Precision	0.07	0.70				

Figure F1. The results from the C and N analysis performed at the iThemba Labs for the harvested material above- and belowground.

G. CLIMATOLOGY DATA

Table G1. Monthly climatology of the Wakkerstroom area, compiled by Moyo (2015). Temperature is from the South African Weather Service (SAWS) municipal station at Volksrust between the years 1904-2012, patched where necessary with data from the SAWS municipal station at Wakkerstroom. SW_{rad} is based on a cloud cover interpolation between SAWS stations which collected sunshine data (Standerton and Newcastle, between the years 1960-1990), fed into a solar geometry radiation model with Ångström equation: $SW_{rad}/SW_{rad,top} = 0.25 + 0.55(\text{SunHours}/\text{MaxSunhours})$. For the locations of the weather stations, see Fig. H2 in Appendix H.

Month	Minimum temperature [°C]	Maximum temperature [°C]	SW_{rad} [MJ·m ⁻² ·day ⁻¹]
January	12.9	25.0	11.89
February	12.5	24.7	10.82
March	11.0	23.5	8.60
April	7.3	21.6	5.87
May	3.0	19.0	3.48
June	-0.3	16.6	2.41
July	-0.5	16.7	3.03
August	2.2	19.4	5.18
September	6.3	22.3	8.00
October	9.3	23.4	10.18
November	11.0	23.8	11.64
December	12.4	25.0	12.26

H. WEATHER STATIONS



Figure H1. The weather station located in Wakkerstroom is marked with a black dot. © Copernicus Sentinel Data (2019).

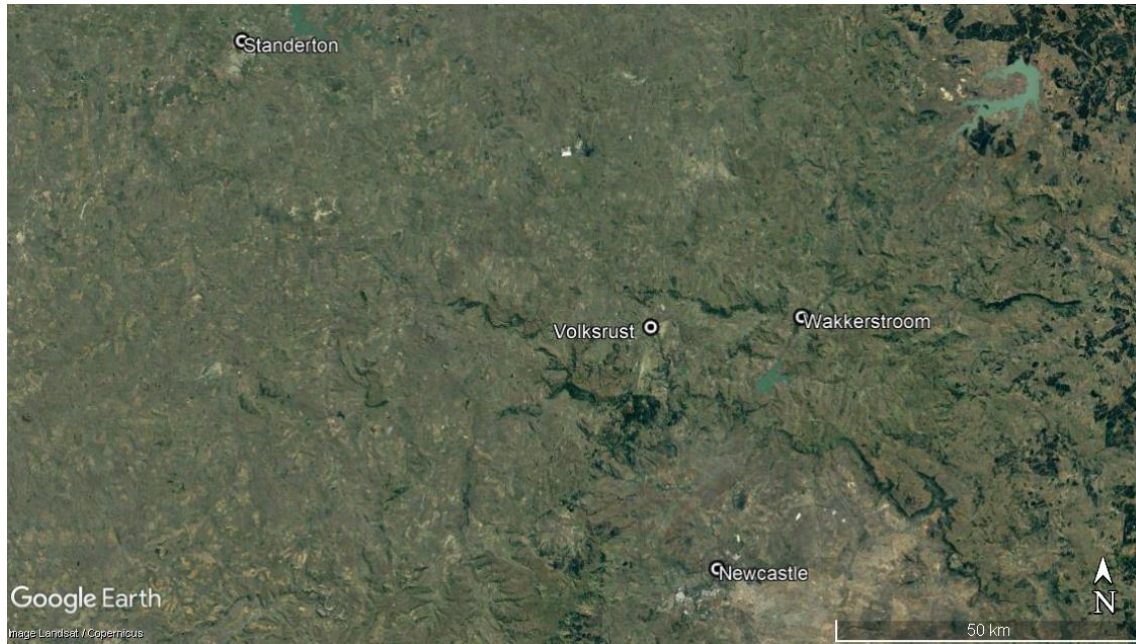


Figure H2. The locations of the weather stations used for the climatology data in relation to Wakkerstroom are Standerton (80 km northwest), Volksrust (25 km west) and Newcastle (50 km south). © Google Earth (2019a).